Master Thesis, Department of Geosciences

Microscopic and organic geochemical characterization of the Lower Carnian black shale interval in the Northern Calcareous Alps (Lunz am See area, Austria)

Palaeoenvironments and source rock potential

Nektaria Panou

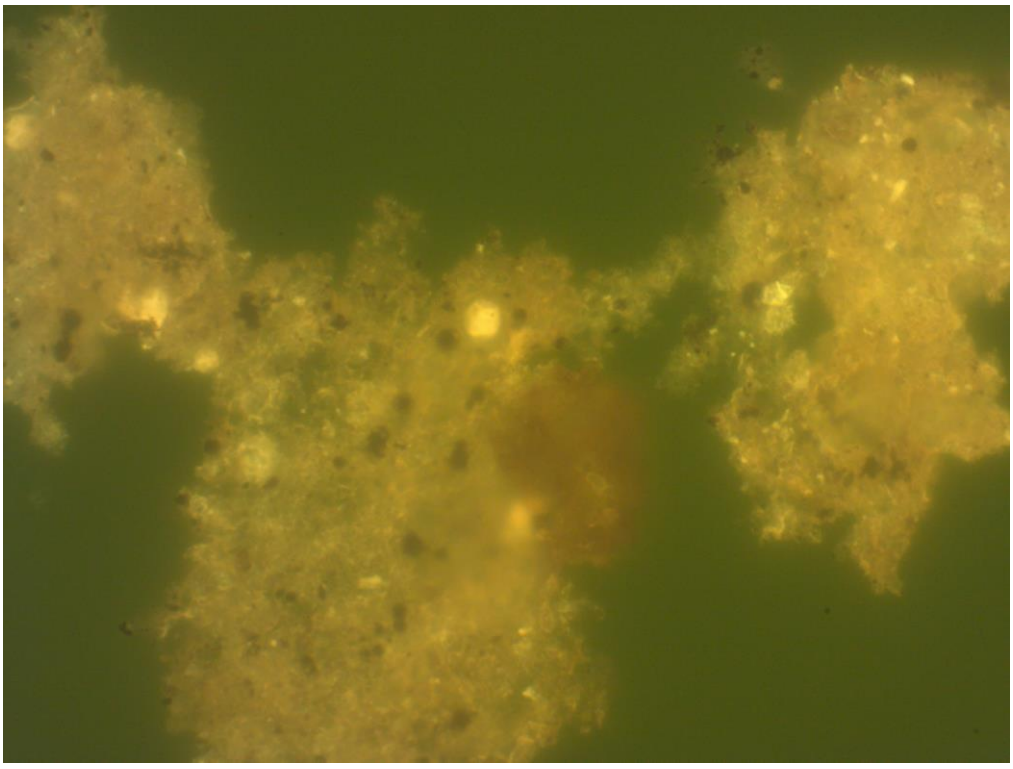

UNIVERSITY OF OSLO

FACULTY OF MATHEMATICS AND NATURAL SCIENCES

Master Thesis, Department of Geosciences

Microscopic and organic geochemical characterization of the Lower Carnian black shale interval in the Northern Calcareous Alps (Lunz am See area, Austria)

Palaeoenvironments and source rock potential

Nektaria Panou

Master Thesis in Geosciences

Discipline: Petroleum Geology and Petroleum Geophysics

Department of Geosciences

Faculty of Mathematics and Natural Sciences

University of Oslo

1/7/2015

UNIVERSITY OF OSLO

FACULTY OF MATHEMATICS AND NATURAL SCIENCES

Front cover illustration: Strongly fluorescent Amorphous Organic Matter (AOM), Reingraben Formation (sample GR12).

This work is published digitally through DUO – Digitale Utgivelser ved UiO

http://www.duo.uio.no

It is also catalogued in BIBSYS (http://www.bibsys.no/english)

Contents

Abstract

At the Julian 1-2, a period major break in reef growth took place in the Tethys realm. This lithological change from carbonates to siliciclastics is interpreted to be the result of increased runoff. Increased continental runoff in turn was related to a period of increased rainfall in the adjacent continental areas and is known as Carnian Pluvial Event (CPE).

Palynofacies analysis and Rock-Eval pyrolysis was performed on sedimentary organic matter extracted from sediments covering the CPE from the outcrops in Lunz am See in Northern Calcareous Alps (NCA) in Austria. Additionally, C-isotope data from bulk sedimentary organic matter and TOC values were integrated from a previous study. The results are used for the reconstruction of the palaeoenvironmental conditions during the black shale formation, the redox conditions and source rock potential. The negative excursion of $\delta^{13}C_{org}$ of the black shale formation in the Carnian is compared with the Rhaetian, which is another negative excursion of $\delta^{13}C_{org}$ within the western Tethys realm.

The sediments were deposited in an epeiric dysoxic-anoxic, neritic shelf with high algae and bacteria productivity. The high productivity was caused by the humid climate during the CPE. Rivers run from Fennoscandinavian hinterland into the NW Tethys margin depositing allochthonous terrestrial matter in the shelf and creating stagnation conditions in the shelf basin. Consequently, the high influx of organic matter and nutrients resulted into eutrophication as algae and bacteria flourish. Furthermore, Rock –Eval pyrolysis reveals kerogen type III and kerogen type IV, but they are generally poor source rock potential due to thickness and maturity and weathering of the organic matter. The CIE is assumed as a good indicator for changes in organic matter.

Keywords: Lunz am See, Austria, Carnian Pluvial Event (CPE), Reingraben Turnover, palynofacies, paleoenvironments, source rock potential.

1. Introduction

Black shales are organic-rich deposits that occur in the marine (less frequently in lacustrine) environment. They represent economically important petroleum source rocks. The formation of the black shales in the Tethys realm during the Late Triassic is not very well understood. It is believed that a change of the geotectonic system or a climate event may have created a global anoxic event.

The western Tethys is characterized by the demise of carbonate platforms and reefs in the Julian, a change in fauna and flora, and an extinction event that influenced conodonts and ammonoids between the Julian to Tuvalian (Hornung et al., 2007a). The main causes for this event are presumably climate warming, humidification and enhanced fresh water runoff, which is also known as the "Carnian Pluvial Event" (Hornung et al., 2007a). The deposition of the Carnian black shales is placed in that period. Black shales of Carnian age are also found in the Southern and Eastern Tethys, Himalaya, Canada and the Arctic realm (Preto and Hinnov, 2003, Hornung et al., 2007a, Hornung et al., 2007b, Keim et al., 2006, Rigo et al., 2007, Xiaofeng et al., 2008, Breda et al., 2009, Preto et al., 2010, Roghi et al., 2010, Rostási et al., 2011, Haas et al., 2012, Lukeneder et al., 2012, Bialik et al., 2013, Arche and López-Gómez, 2014, Nakada et al., 2014).

1.1 Aims and objectives

This study deals with a black shale event in the Late Triassic (Carnian) spans the uppermost Reifling Formation, Göstling Member and the Reingraben Formation and is located at the transition between the Julian 1- Julian 2 stages of the Carnian. A geochemical analysis including total organic carbon (TOC) and bulk carbon isotope values and other geochemical proxies has been carried out (S. Mueller, PhD project, published in Mueller et al. (2015)). The bulk carbon isotope values, which are rather insensitive to diagenetic alterations (Korte et al., 2005), correlate with areas with different facies (Hornung et al.,

2007b). Results show a sudden increase in TOC and decrease in carbon isotope values. The Göstling Member has some intervals with TOC values ranging from 15-20%. The TOC for the Reingraben Formation has values ranging between 0.5-5.4%. The carbon isotope values have negative excursion in Göstling Member while the Reingraben Formation has relatively more positive values.

This study is conducted to shed new light on the depositional environment of Göstling Member and Reingraben Formation and reveal associated climate and environmental changes, in particular tackling the following research questions:

1. What is the microscopic composition of the organic matter?
2. What is the depositional environment (redox conditions) on the Western Tethys shelf during the interval of the Göstling Member and the Reingraben Formation?
3. What is the source rock potential of the black shales?

The study is in close collaboration with a current PhD project at the Geoscience Department at University of Oslo, Norway. The PhD project is conducted by PhD student Steven Mueller and supervised by Prof. Wolfram Michael Kürschner. Steven Mueller provides the palynological slides of the samples used in the present thesis, as well as the results from $\delta^{13}C_{org}$ and TOC.

1.2 Approaches to thesis

The present thesis uses figures, tables and diagrams with the purpose theory and results to be pleasant and perceptual in readers. As stated in (Winn, 1993) the main difference in searching between a text and a diagram is that in the second case the early stages of search are guided perceptually. The meaning of depicting symbols and the way they are defined are purposely for the reader, guiding followed search. The symbol systems and conventions of diagrams are principally dimensional and these are dynamic factors in directing search. The knowledge of the content of the diagram helps the reader what to look for next and in occasions even where to search for it. The interaction of diagrams use, readers´ knowledge,

and the aims of search sets search strategies. These strategies, when applied successfully, drive the reader to meet the targets of extracting and reminding information to which the search leads.

1.3 Background

1.3.1 Paleoclimatology

The drift of the continents is responsible for the climate over the geological history of Earth. According to (Kutzbach and Gallimore, 1989), the Triassic climate for Laurasia and Gondwana was continental, with hot summers, cold winters and large- scale summer and winter monsoon circulations. The western tropical coasts, east coasts and regions around 40° latitude experienced seasonally arid conditions. Distinguishing of climate zones is difficult owing to the intense monsoonal system which was possible stronger than the present monsoonal system (Wang, 2009, Preto et al., 2010).

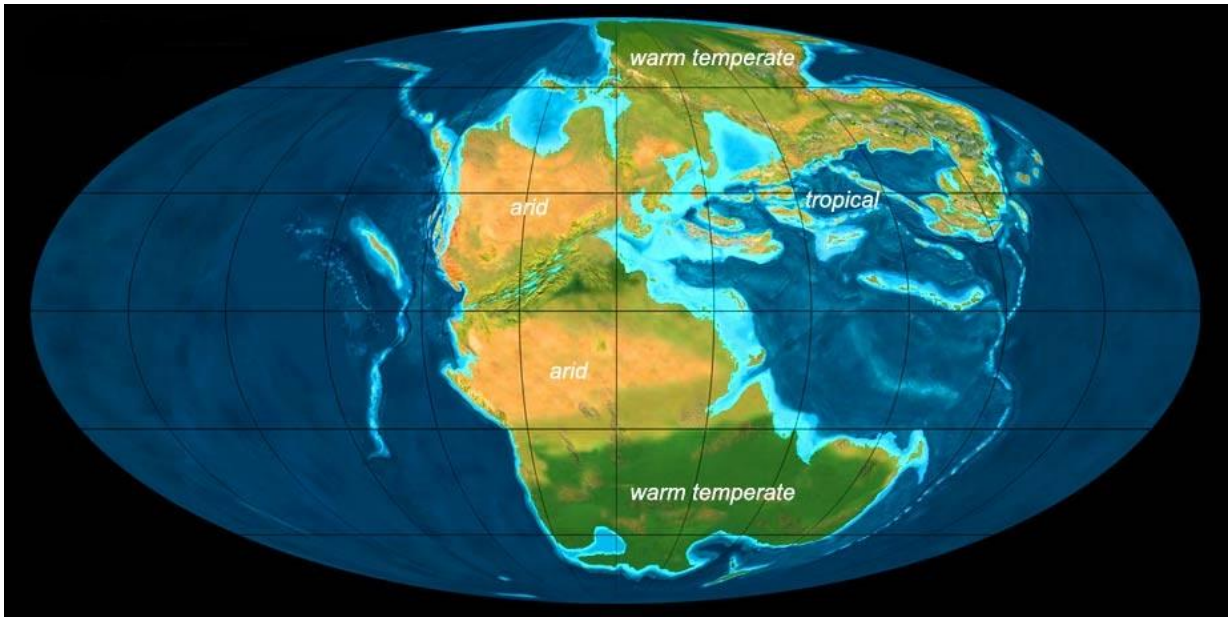

Fig. 1.1: The Upper Triassic climate and the distribution of climatic zones. Credit: Dr Ron Blakey, NAU Geology.

The Tethys domain was mostly affected by a Late Triassic intense, global monsoonal system (Robinson, 1973, Wang, 2009, Preto et al., 2010). The large landmasses during that period can be approximately divided into three climatic regions of non-zonal pattern owing to the monsoonal atmospheric circulation (Fig. 2.4). According to Parrish and Peterson (1988) and Mutti and Weissert (1995), the western Tethys, positioning among the two tropics latitudes and subtropical highs, had dry climate all over the entire year. The eastern coasts of Laurasia and Gondwana and the coasts west of Pangea would have undergone into an alteration of wet and dry seasons. On the contrary, the high latitudes were possibly influenced by westerlies and polar easterlies assuming wet climate with warm climate palaeosols and floras to have indicated latitudes up to 85° (Robinson, 1973, Kidder and Worsley, 2004). The modelling study of Sellwood and Valdes (2006) shows the non-latitudinal distribution of climate zones with considerable differences of the climates' distribution. However, the western Tethys area was stigmatized by strong seasonal monsoon but not from an arid climate.

Olsen and Kent (2000) were noticed a zonal climatic pattern all over the Atlantic rift basins of eastern North America with narrow equatorial humid zone and an arid belt continuing into humid temperate climates in the north. The low pressure zone of the Tethys pulls air masses from Eastern Panthalassa straight away to western Pangea of the mega monsoonal regime which is connected with a humid equator in the Atlantic rift basins area (Parrish, 1993). Many studies denote the effect of monsoonal circulation on Pangea at the tropical latitudes (Dubiel et al., 1991, Mutti and Weissert, 1995, Spalletti et al., 2003, Loope et al., 2004), yet there is a minor evidence of climatic alterability. Nonetheless, the conspicuous episode of strong humid conditions at the Julian 1-Julian 2 boundary typifies a significant proof. This episode, the so called Carnian Pluvial Event (CPE), was accompanied by a biotic turnover and environmental changes (Simms and Ruffell, 1989, Simms et al., 1995, Preto et al., 2010). It has been recognized in many regions such as the Germanic Basin and the Northern Calcareous Alps (Schlager and Schöllnberger, 1974) and is detected from the demise of carbonate platform and the input of siliciclastics in the western Tethys. Hygrophytic palynological assemblages as well as different aspects of the siliciclastic input have been taken into consideration for concluding a temporary change to wetter climate (SIMMS and RUFFELL, 1990, Simms et al., 1995).

After the Carnian Pluvial Event, the climate shifted back to hot and semi-arid conditions as indicated by the deposition of Dolomia Principale succession (Haas and Demény, 2002). It is characterized by dolomitized peritidal carbonates. Nevertheless, Hallam (1985) recorded a shift to more humid conditions in the early Rheatian.

Dramatic climate change was denoted across the Triassic- Jurassic boundary that included a devastating mass extinction followed by a biotic turnover (Preto et al., 2010). A possible cause could be the activation of the Central Atlantic Magmatic Province accompanied by high volcanic emissions (Marzoli et al., 2004, Preto et al., 2010). A greenhouse to hot- house climate was assumed as the major extinction causation (McElwain et al., 1999, Hesselbo et al., 2002, McElwain and Punyasena, 2007). The existence of kaolinite- rich boundary clays in NW Europe together with isotope geochemistry data show strong weathering in a hot, humid climate (Korte et al., 2009). In addition, the loss of seed fern *Dicroidium* and the peltasperm group, mainly close to the marine realm, represents evidence of the end- Triassic mass extinction and the cause of their demise is the short- lived cooling and acid rain which provoked by volcanic SO_2 fluxes (Van de Schootbrugge et al., 2009). Generally, climatic changes followed by floral extinctions are more conspicuous in NW Europe and NE North America, where the Central Atlantic volcanism was more intense (Hallam and Wignall, 1999). The Late Triassic and Early Jurassic sequences in Brazil and Argentina indicate more dry conditions and this can be caused by the continental drift from south temperate regions into the southern arid belt (Olsen and Kent, 2000).

1.3.2 Palynoflora

The early Carnian to Norian was characterized by a decrease in palynoflora diversity of about 50%, which coincided with a decrease in the number of pollen and spore species (Kürschner and Herngreen, 2010). A biotic turnover in both terrestrial and marine realms has been suggested by Simms and Ruffell (1989), which coincides with the proposed climatic change. Coniferalean and pteridosperm affinities were the most common flora located in the uplands (Fig. 1.2) (Roghi et al., 2010).

Fig. 1.2: Typical Triassic palynoflora. The picture was taken from: http://www.bbc.co.uk/nature/history_of_the_earth/Triassic (Credit: John Sibbick)

Roghi et al. (2010) and Mueller et al. (2015) classified the sporomorphs into hygrophytes and xerophytes related to climatic conditions (Table 1.1). Hygrophytes are characterized by, for example, the *Aulisporites astigmoses* and *Lagenella martinii* assemblages (Roghi et al., 2010). These forms are found in Europe and Middle East localities suggesting a humid climate perturbation in the northern hemisphere from tropical to high latitudes (Roghi et al., 2010).

According to many authors (Roghi et al., 2010, Mueller et al., 2015), poor microflora present in uppermost Reifling Formation and Göstling Member such as *Ovalipollis*, *Triadispora* and *Concavisporites* sp., while marine specimens are represented by algae *Tasmanites* spp., *Micrhystridium* spp., *Cymatiosphaera* spp. and *Botryococcus* spp. Mueller et al. (2015) observed an increase in the spore to pollen ration the top of the Göstling Member and within the section at Grossreifling. This interval is characterized by *Ovalipollis*

spp., *Triadispora* sp. (bisaccate pollen), *Aratrisporites* spp., *Enzonalasporites vigens* and *Partitisporites* spp. However, abundance of bisaccate pollen decreases.

An *Aulisporites-Cycadopites* assemblage zone has been recognized in the Reingraben Formation (Mueller et al., 2015). It is based on the first occurrence of *Aulisporites astigmosus*, an increase in *Cycadopites* spp. and fall decrease of *Enzonalasporites vigens* and *Partitisporites* spp. Bisaccate pollen such as increases *Lunatisporites* spp. and *Ovalipollis* spp. increase. Additionally, the aquatic signal in the Reingraben Formation consists of foraminiferal test linings and the algae Micrhystridium spp., *Cymatiosphaera* spp. and Botryococcus spp..

Table 1.1: The morphospecies group and their palaeobotanical and environmental interpretation , modified after Roghi et al. (2010).

Morphospecies group	Paleobotanical affinity	Environmental interpretation
Azonotriletes	Equisetophytic and pteridophytic	Hygrophytic, swamps or marshes
Zonotriletes	Lycopodiophytic	Hygrophytic
Cavatomonoletes	Lycopodiophytic	Hygrophytic
Azonomonoletes	Pteridophytic	Hygrophytic, swamps or marshes
Aulisporites astigmosus	Cycadeoidales; Bennettitales Kräusel and Schaarschmidt (1966)	Hygrophytic
Monosulcate	*Cycadopites* (Bennettitales, Cycadales and Ginkgoopsida); Palyssiaceae (Cephalotaxaceae, Conifers);	Hygrophytic
Porcellispora sp.	Bryophyte	Xerophytic; Reinhardt and Ricken (2000)
Monosaccate	Coniferalean	?Xerophytic
Bisaccate	Coniferalean and pteridosperm	Xerophytic
Taeniate pollen	Coniferalean	Xerophytic
Ovalipollis spp.	Coniferalean	Xerophytic
Triadispora spp.	Coniferalean	Xerophytic
Camerosporites spp.	Coniferalean (Cheirolepidiaceae)	Xerophytic
Circumpolles	Coniferalean (Cheirolepidiaceae)	Xerophytic
Alete pollen grains	Coniferalean	Xerophytic
Polyplicates	*Dechellya gormanii* (*incertae sedis*, Ash, 1972)	Xerophytic
Acritarchs	Acritarcha	Open marine
Algae	Green Algae, Clorophytes	Freshwater to intertidal shallow marine

2. Geological setting

2.1 Location

The investigated sections are located around Lunz am See, in the Northern Calcareous Alps (NCA) in Austria, approximately 100 km west of Vienna (Fig. 2.1). The sample material was taken from 4 study sections around Lunz am See. These 4 sections and their coordinates are (see Fig. 2.1) (Mueller et al., 2015):

Steinbach (STB)	N47°48.354' E014°57.006'
Grossreifling (GR)	N47°39.636' E014°43.686'
Sulzbachgraben-2 (SBG-2)	N47°52.290' E014°59.509'
Mendlingsbach (ME)	N47°45.050' E014°52.353'

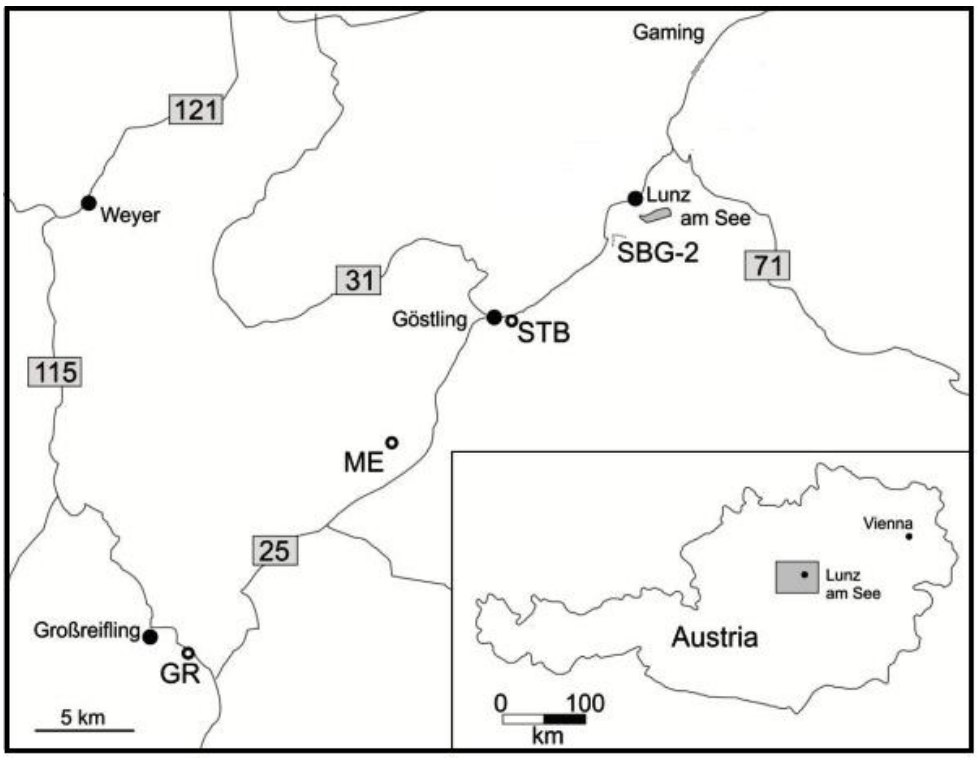

Fig. 2.1: Location of the study area (modified after Mueller et al., 2015).

2.2 Regional geology

The investigated area was created by the rearrangement of tectonic plates (Fig. 2.2). The Cimmerian micro-continents drifted northward from Gondwana towards Laurasia and closed the Paleaotethys while Neotethys opened behind them (Sengör and Hsü, 1984, Sengor and Natalin, 1996, Golonka, 2004, Soua, 2014). The Palaeotethys `s closure is the main global tectonic event of the Triassic (Golonka, 2007). The onset of rifting and break- up of Pangaea was in the Early Triassic and continued and became more intense in the Early Norian (Ziegler and Maatschappij's-Gravenhage, 1982, Ziegler, 1988, Withjack et al., 1998, Golonka and Ford, 2000, Golonka, 2002, Veevers, 2004, Golonka, 2007).

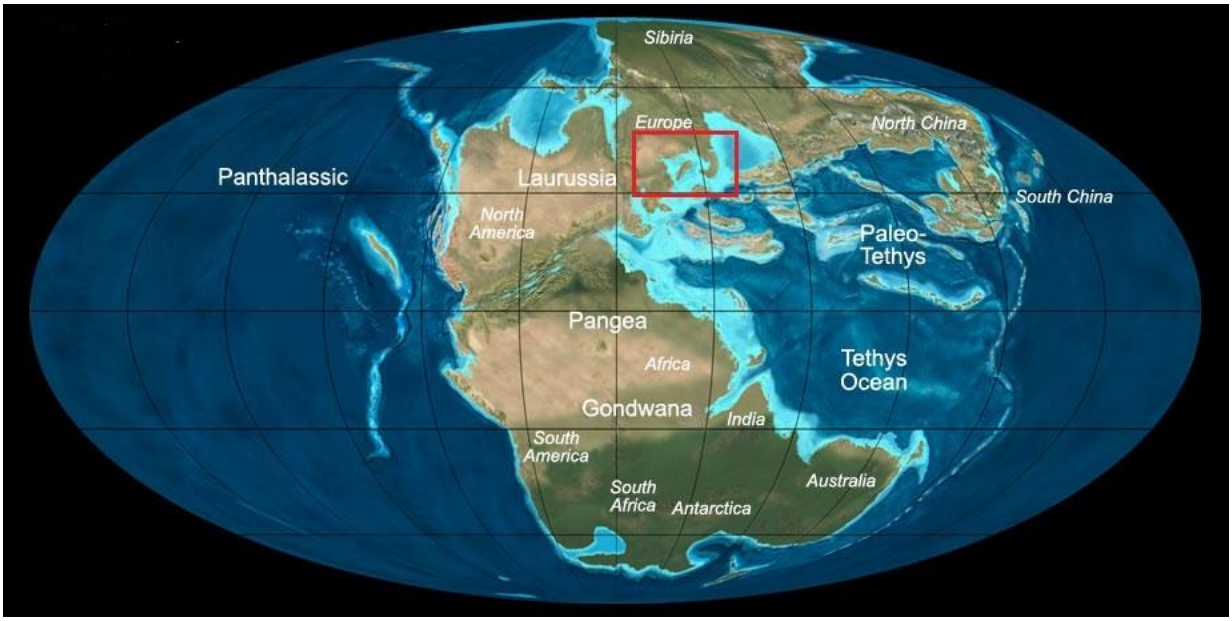

Fig. 2.2: Global plate tectonic map of the Late Triassic (220 Ma). The red square indicates the study area. Credit: Dr Ron Blakey, NAU Geology.

Laurasia and Gondwana started to separate during the Early Triassic and continued throughout the rifting phase of the Late Triassic (Golonka, 2007). The Cimmerian plates disintegrated from Gondwana and moved northward to Laurasia during Late Paleozoic-Triassic. Simultaneously, the Palaeotethys closure took place (Şengör, 1984). Due to this closure, Palaeotethys oceanic crust was consumed and the Neotethys Ocean opened (Golonka, 2007). In the western Tethys area, several Cimmerian microplates (Sengor and Natalin, 1996, Şengör, 1984) collided to the Eurasian margin(Zonenshaĭn et al., 1990,

Golonka, 2004, Golonka, 2007). The Northern Calcareous Alps (NCA) formed a marginal platform in Europe (Golonka, 2007).

Due to the Alpine Orogeny, in the Cenozoic, the Mesozoic sediments of the NCA underwent several stages of deformation, including folding and thrusting, during Late Jurassic to Tertiary times. This created a nappe complex which reposes with overthrust contact on the Rhenodanubian Flysch Zone in the north and on Variscan basement in the south (Mandl, 2000). The succession of nappes from north to south and from bottom to top consists of: Bajuvaric nappes, which are the northern frontal part of NCA, with synclines and anticlines having a narrow shape. The overlying Tyrolic nappe complex, which includes the dolomites, shows internal thrusting and faulting with slightly folding. The Juvavic nappes, which overly the Tyrolic nappes, is the uppermost tectonic element (Mandl, 2000)(Fig. 2.3). In Permo- Triassic times the NCA were a passive continental margin. They were created onto the Veriscan basement, in Pangaea, owing to rifting and spreading of the Tethys.

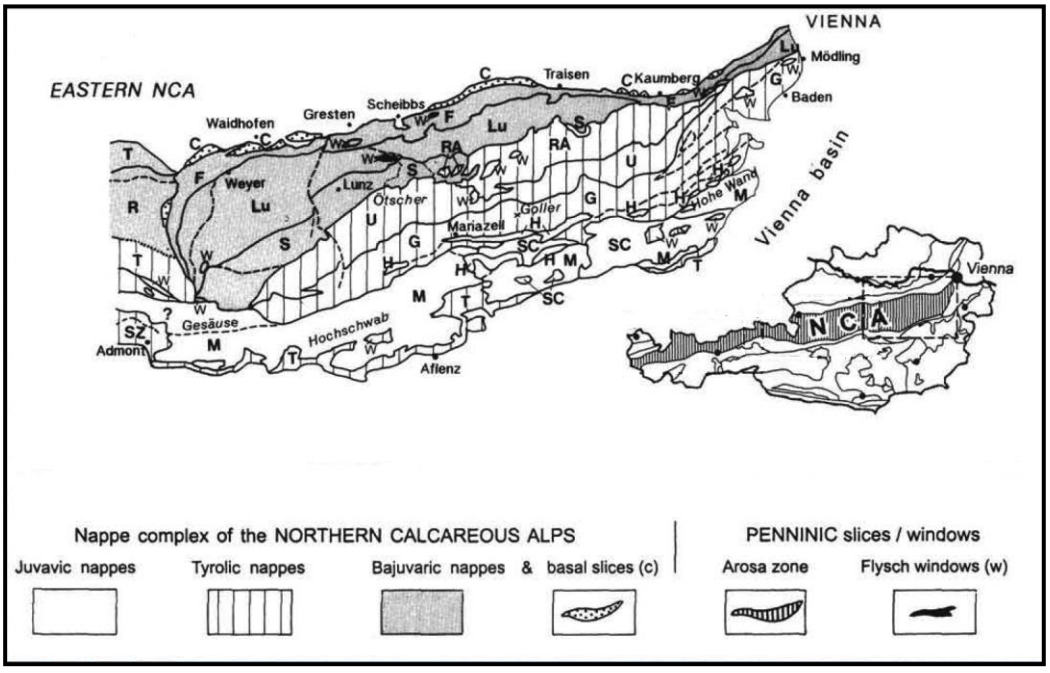

Fig. 2.3: The nappe complexes of the Eastern NCA (Mandl, 1999).

2.3 Sedimentary environments

In the Carnian, the Lunz am See area succession represented an intraplatform basinal setting in a shallow shelf at the NW Tethyan passive margin (Hornung et al., 2007a, Hornung et al., 2007c). In early the Julian 1, the rimmed platform fed the basin depositing the basinal limestones (Reifling Formation) (Fig. 2.4 a). In the Julian 1, the onset of Carnian Pluvial Event coincided with a drop in sea-level (Fig. 2.4b) (Jacquin, 1998, Keim et al., 2001). The platform demise started when periplatform–mud with reefal influence (*Tubiphytes*) deposited in a deep and low–energy setting (Göstling Member) (Hornung and Brandner, 2005) . The fresh water caused nutrient excess and oxygen depletion due to eutrophication (Hornung et al., 2007a). In the Julian 2, the oxygen supply decreases more, indicating a dysaerobic setting. Then, a massive river system running from Fennoscandian Craton across most of Western Europe deposited large volumes of siliciclastic sediments into the shallow shelfs leading to a drowning of the carbonate platforms (Arche and López-Gómez, 2014). The high terrigenous influx and very low carbonate supply resulted in an almost restricted anoxic setting (Fig. 2.4c) (Hornung and Brandner, 2005). This sedimentological change in the Western Tethys region of the Northern Calcareous Alps is regionally also known as the Reingraben Turnover (Schlager and Schöllnberger, 1974, Breda et al., 2009). The siliciclastic input reaches its peak with the deposition of the Lunz Formation consisting of deltaic sandstones and siltstones (Fig. 2.4d) (Mueller et al., 2015). In the Tuvalian, the carbonate platform production recovered (Fig. 2.4e).

Similarly, anoxic basinal environments along the NW Tethys margin have been observed in the Hallstatt deep swells and Partnach intraplatform basin facies at locations in southern Germany (Hornung and Brandner, 2005, Hornung et al., 2007a, Hornung et al., 2007c).

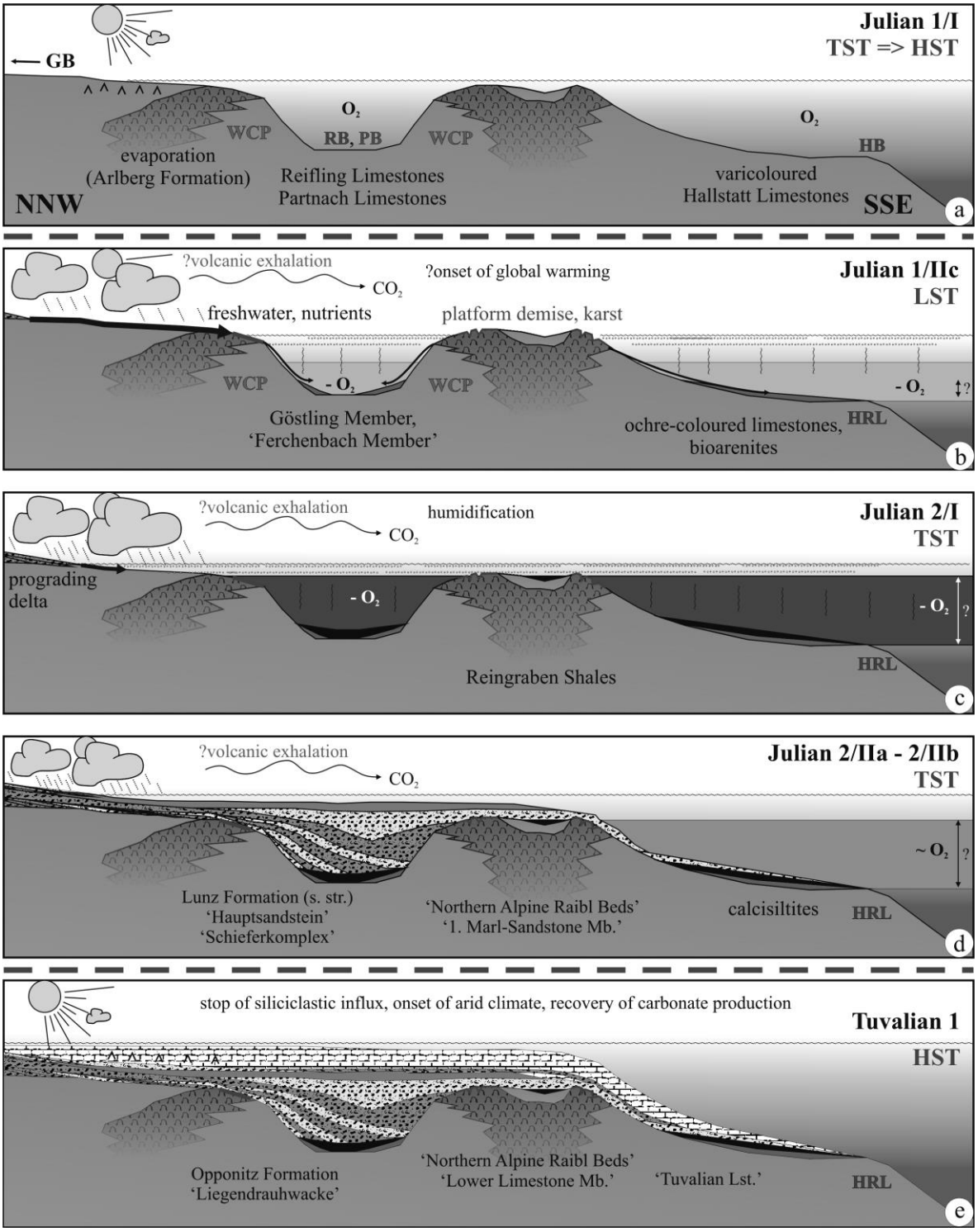

Fig. 2.4: Schematic cross-section through shallow-marine NW Tethyan environment (Hornung et al., 2007a). The a-e stages represent the evolution of sedimentary environments from the Julian to the Tuvalian.

2.4 Lithostratigraphy

The studied sequence is cropping out at Steinbach, Grossreifling and Ahorngraben in the Lunz am See area. The sections compose a lithostratigraphical succession from the lowermost Reifling Formation to the uppermost Reingraben Formation (Fig. 2.4), as indicated below (Hornung et al., 2005):

Reifling Formation (Julian 1)

This formation consists of greyish-coloured filament- wackestones including algal crusts of detritical reefal (*Tubiphytes*), peloids, ostracods, gastropods and pelagic components such as filaments(Hornung and Brandner, 2005).

Göstling Member (Julian 2/1)

This Member is a calciturbidic, radiolarian- rich limestones (Hornung et al., 2007b). In more detail, it contains dark grey-coloured pyrite flaser grainstones in the lower part and bioclastic mudstones in the upper (Hornung and Brandner, 2005, Hornung et al., 2007c).

Reingraben Formation (Julian 2/1)

This formation consists of dark greyish to dark unfossiliferous shales. The lower and middle part contains few calcareous intercalations of borrowed biogenic wackestones, while upwards are unfossiliferous thinly laminated mudstones and marls (Hornung and Brandner, 2005).

The Carnian lithostratigraphy from the area of Spiti Himalaya (Northern India) shows similarities with the lithostratigraphy at Lunz am See. However, the Spiti area succession does not contain the calciturbidic limestones of Lunz am Sea (Hornung et al., 2007b). The Hallstatt facies lithostratigraphy show slight differences from the studied succession lithostratigraphy, too. According to Mandl (2000) and Hornung and Brandner (2005), the Hallstatt succession consists from bedded grey limestones (Reifling Formation), green marly limestones, dark grey limestones (Göstling Member), ochre-coloured limestones that are overlain by the shales of the Reingraben Formation.

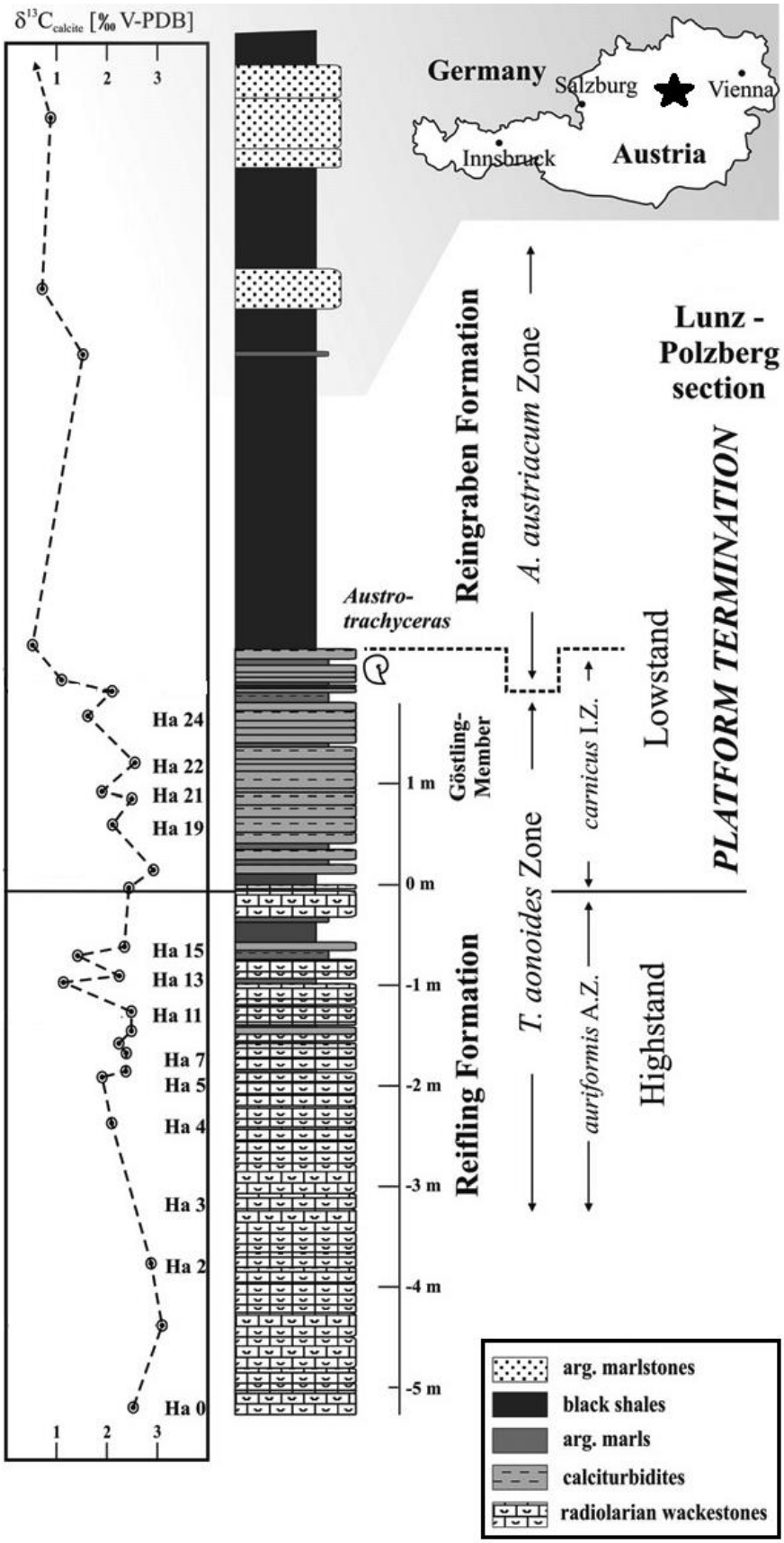

Fig. 2.4: Lithostratigraphy of the austroalpine facies as exposed in Lower Austria and the $\delta^{13}C_{calcite}$ response (Hornung et al., 2007b).

2.5 Biostratigraphy

Many authors have referred to global ammonite and conodont biochronology that define different bioprovinces (Krystyn, 1980, Gallet et al., 1994, Krystyn et al., 2002, Hornung et al., 2007c, Roghi et al., 2010).

According to ammonite zonation (Krystyn, 1980, Kozur, 2003, Hornung et al., 2007c) the upper Reifling Formation corresponds to the *Trachyceras aonoides* ammonoid zone of Julian 1-II age, while Göstling Member and Reingraben Formation correspond to the *Austrotrachyceras austriacum* ammonoid zone of Julian 2-I age (Fig. 2.5).

Analysis of conodont faunas defines conodont zones which coincide with chronical periods of the lithological units(Fig.2.5) (Hornung et al., 2005). In the limestones of the Reingraben Turnover, the abundance of well-preserved conodonts contributes to the biostratigraphic zonation (Hornung and Brandner, 2005). The bedded grey limestones are characterized by *G. polygnathiformis* (Budurov and Stefanov, 1965). The age is defined as Langobardian-Julian 1. The conodont assemblage zone of *G. mostleri* is of Julian 1, while *G. tadpole* occurs in the Julian 2. The *G. tethydis* (Krystyn, 1980, Krystyn, 1983) conodont assemblage zone is found in the Reingraben Formation and indicates Julian 2.

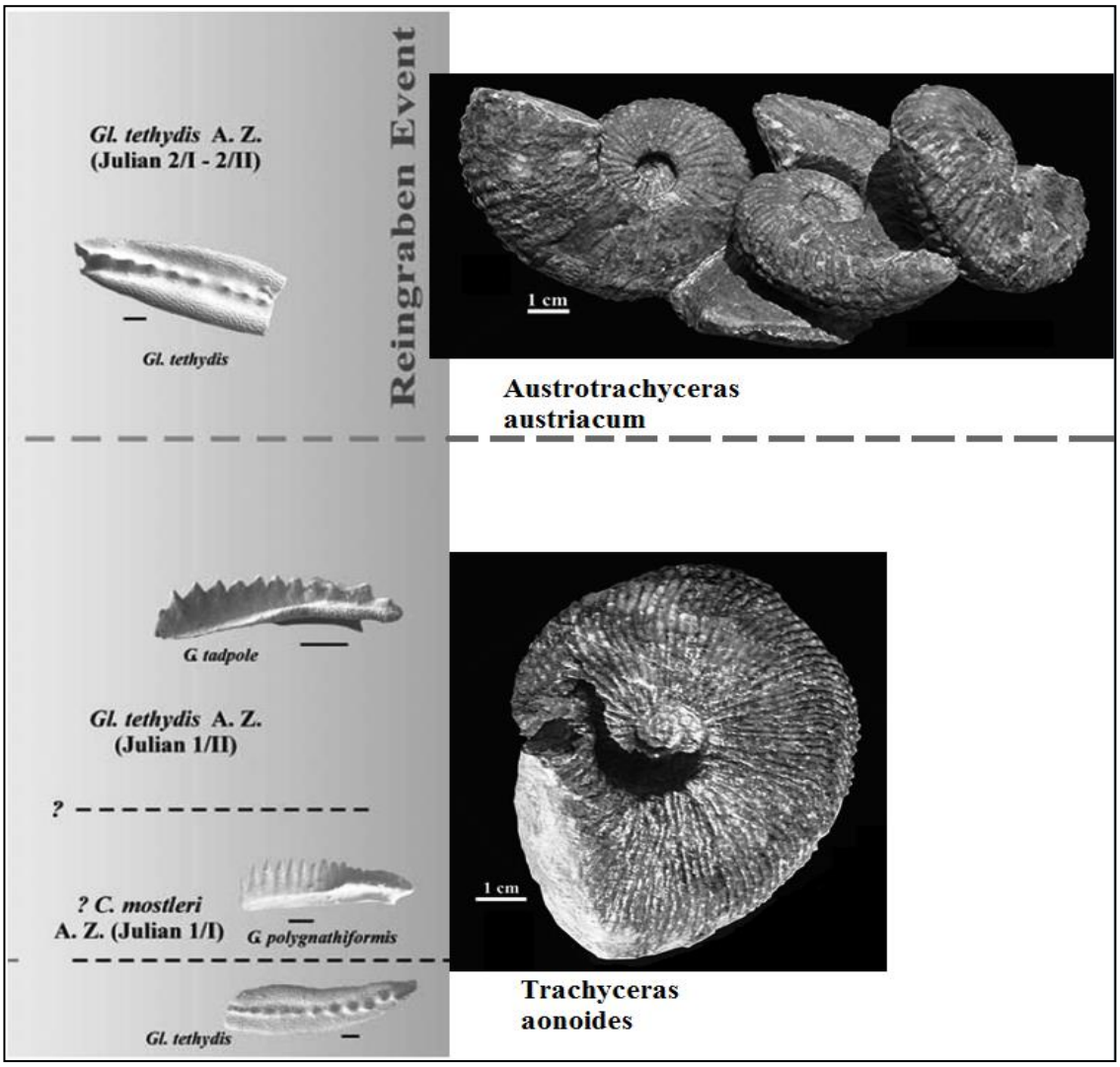

Fig. 2.5: Conodont and ammonite biostratigraphy according to Krystyn (1980) and Krystyn (1983), modified after Hornung and Brandner (2005) and Hornung et al. (2007c).

3. Material and methods

3.1 Samples

The studied sections from the Lunz am See area were selected due to their excellent exposure of the Reingraben Turnover in the Northern Calcareous Alps. The investigation of the Reingraben Turnover is part of a research project addressing changes in the Late Triassic climate worldwide. The significance lies upon the similarity of Carnian sediments of Tethys Sea (e.g. in Tunisia, Himalaya and Southern Alps) (Preto and Hinnov, 2003, Hornung et al., 2007b, Soua, 2014) which is characterized by a high abundance of AOM and an increase of TOC during Julian 1-2.

Samples were acquired, mostly, from road cuts in Steinbach, Grossreifling and Ahorngraben locations by S. Mueller, W. M. Kürschner (both University of Oslo) and L. Krystyn (University of Vienna) during a field campaign in 2014). In the present study, the palynological analysis has been carried out on 18 samples. Two of them (STB1, GR1) contain high amounts of amorphous organic matter (AOM) (see Appendix A for full list of samples). Furthermore, Rock-Eval pyrolysis was carried out on 28 samples (see Appendix B for full list of samples).

3.2 Palynological slide preparation

Palynological processing and slide preparation was done by S. Mueller at the Laboratory of Palynology at the Department of Geoscience of University of Oslo, Norway. Quantitative methods according to standard procedures were used for the processing. Sediments with a weight between 5-10 g were slightly crushed (≥5mm≥), while afterwards a specific amount of *Lycopodium* marker spores was added in the mixture. *Lycopodium* is a marker spore that is used for determining the quality of the palynomorphs assemblages.

The samples were treated, firstly, with 10% HCl, then HF and followed by HCl (30%) and neutralized for dissolution of carbonates. The process continued and the samples were treated with HF, then HCl (30%) and finally neutralized. This treatment removed silicates. Finally, the residue was washed with water until neutral pH and sieved with a 15 and 250 μm mesh (Kuerschner et al., 2007, Traverse, 2007, Mueller et al., 2014). Heavy liquid separation was done in order to remove heavy minerals (e.g. pyrite). The sample residue was then mounted on microscopic slides.

3.3 Bulk $\delta^{13}C_{org}$ analysis

All 18 samples were analyzed for their bulk $\delta^{13}C_{org}$ isotope composition. Sediment weighing 1 g was crushed and treated with 15 ml of 1 M HCl to remove the inorganic carbon (Kuerschner et al., 2007, Bonis et al., 2009, Mueller et al., 2014). The measurement of carbon-isotope ratios was done on homogenized samples by a Europe Scientific 20-20 IRMS Elemental Analyzer–Isotope Ratio Mass Spectrometer (EA–IRMS), by Iso Analytical Ltd, The Quantum, United Kingdom. Analytical precision based on routine analysis of internal laboratory reference materials shows a standard deviation of <0.08‰ for the bulk carbon isotope values (Mueller et al., 2015). The reference material IA-R001, wheat flour was used ($\delta^{13}C_{V\text{-}PDB}$ = -26.43‰). Results are reported using standard delta notation Vienna PDB.

3.4 Rock-Eval analysis

All samples were analyzed by the Rock-Eval method. The procedure follows Espitalie et al. (1985), Espitalié (1986) and Peters (1986). The sample material was finely grounded with an automated Herzog grinder. About 80 μg of ground sample are weighed into a pyrolysis crucible and then heated to 200 °C to determine the amount of free hydrocarbons (free HC, S1). Subsequently, the amount of pyrolysable hydrocarbons (S2) is measured when the sample is heated in an inert atmosphere (N_2) from 200 °C to 600 °C at a heating rate of 25 °C/minute. The S1 and S2 are reported in mg HC/g sample. Additionally, the generated CO and CO_2 are measured during this pyrolysis stage and the subsequent oxidation stage by an infrared detector.

The parameters that were derived from the Rock-Eval measurements reflect the thermal maturity and hydrocarbon generation potential of source rocks. Table 3.1 referred to the measured and derived parameters and their significance. The measurements were carried out at the laboratory of Deltares (Utrecht, The Netherlands).

Table 3.1: An overview of measured and derived parameters of Rock-Eval pyrolysis.

Measured parameters			
	Detector/Oven	**Unit**	**Name**
S1	FID/Pyrolysis	mg HC/g rock	Free hydrocarbons
S2	FID/Pyrolysis	mg HC/g rock	Oil potential
TpS2	TC/Pyrolysis	ºC	Temperature at maximum of S2 peak
S3	IR/Pyrolysis	mg CO_2/g rock	CO_2 from organic source
S3'	IR/Pyrolysis	mg CO_2/g rock	CO_2 from mineral source
S3CO	IR/Pyrolysis	mg CO/g rock	CO from organic source
S3'CO	IR/Pyrolysis	mg CO/g rock	CO from mineral source
S4CO	IR/Oxidation	mg CO/g rock	CO from organic source
$S4CO_2$	IR/Oxidation	mg CO_2/g rock	CO_2 from organic source
S5	IR/Oxidation	mg CO_2/g rock	CO_2 from mineral source
Derived parameters			
	Unit	**Formula**	**Name**
Tmax	ºC	TpS2-STD Tmax	Tmax (actual measured Rock Eval VI value converted to Rock Eval II value)
PI		S1/(S1+S2)	Production Index
PC	% weight	$\frac{[(S1+S2)x0.83]+\left[S3x\frac{12}{44}\right]+\left[\left(S3CO+\frac{S3'CO}{2}\right)x\frac{12}{28}\right]}{10}$	Pyrolysable Carbon
RC CO	% weight	(S4CO x 12/44)/10	Residual Carbon CO
RC CO_2	% weight	($S4CO_2$ x 12/44)/10	Residual Carbon CO_2
RC	% weight	RC CO + RC CO_2	Residual Carbon
TOC	% weight	PC + RC	Total Organic Carbon
HI	mg HC/g TOC	(S2 x 100)/TOC	Hydrogen Index
OI	mg CO_2/g TOC	(S3 x 100)/TOC	Oxygen Index

3.5 Palynofacies

The organic particles of palynomorphs and palynodebris were counted of approximately 300 items per slide. The categorization of the organic particles is according to Tyson (1995), Batten (1996) and Traverse (2007) (Table 3.2).

All 18 samples from the Grossreifling, Steinbach and Sulzbachgraben-2 sections were examined under transmitted and fluorescence light microscopy. Countings were carried out using transmitted light of the model Nikon Optiphot microscope (Japan). The magnification used for the observation of the individual organic particles is ×40. A fluorescence light Leitz Diaplan microscope (Germany) was used for observations upon the preservation state of palynomorphs and AOM (Tyson, 1995). The magnification used for the observation of the individual organic particles is ×20, while for highly accuracy ×40 was used and oil immersion. Photos were taken with an AxioCam ERc 5s camera connected to a computer using software Zen 2011.

The presentation of components can be either as relative (%) or as absolute (g^{-1}) abundance. In the present study, the relative abundance it is used which represent the components' percentage of the total sum.

The calculation and plotting of the relative abundances were carried out using software Tilia (Grimm, 1991-2011) and Microsoft Excel, while figures and graphs were worked out by Adobe Illustrator and Microsoft Paint.

Table 3.2: Classification of microscopic sedimentary organic matter (POM) (Traverse, 2007).

I. Palynomorphs-proper (PP)

A. Plant-related remains
1. **Spores (F)**
   a. **Megaspores (> 200µm)**
   b. **Small spores (≤ 200µm)**
2. **Pollen (F)**
3. **Green algae (F)**
   a. **Hydrodictyaceae coenobia**
   b. **Zygnemataceae zygotic spores**
   c. **Prasinophyceae zoospores**

B. Acritarchs (F)

C. Dinoflagellate cysts (F)

D. Cyanobacteria (rare as palynomorphs)

E. Animal-related remains (= "zoomorphs")
1. **Foraminiferal chitinous linings**
2. **Chitinozoans**
3. **Scolecodonts**
4. **Insect discrete exoskeleton parts**
5. **Tintinnids, other miscellaneous animal groups**

F. Fungal spores and sclerotia

G. Indeterminate and opaque palynomorphs

II. Palynodebris (PD)

A. Structured organic matter (STOM) = ca. Particulate organic matter (POM)
1. **Phytoclasts**
   a. **Wood**
   b. **Cork and bark**
   c. **Charcoal**
   d. **Cuticles (F)**
   e. **Other plant tissues**
   f. **Coal maceral fragments, including vitrinite**
2. **Zooclasts: fragments of arthropod exoskeletons, etc.**

B. Unstructured (= without structure) organic matter (USTOM)
1. **Amorphous organic matter (AOM)**
   a. **Of terrestrial origin (AOMT)**
   b. **Of aquatic origin (AOMA) (F)**
   c. **Undifferentiated gelified matter**
2. **Unstructured with identifiable characteristics**
   a. **Resin, including amber (F)**
   b. **Bitumen**

3.6 Palynofacies Analysis

Combaz (1964) introduces palynofacies as the distinctive total assemblage of all particulate organic matter (POM) that is observed in the microscope. However, many authors used different definitions, such as "organic matter"(Lorente, 1990), "palynoderbris" (Van der Zwan, 1990, Traverse, 2007) and "kerogen" (Tyson, 1995). In this study, the classification of the different constituents of kerogen is based on the three authors' approaches and is indicated in Table 3. Additionally, analytical description of each group and its constituents in the present work, it is shown in Table 3.3.

Table 3.3: Classification of kerogen and its descriptions (Tyson, 1995, Batten, 1996, Traverse, 2007).

	GROUP		CONSTITUENT	CHARACTERISTICS	SIZE (µm)
STRUCTURELESS	AOM		Heterogeneous	Granular with numerous inclusions (pyrite, small remains from sporomorphs and phytoclasts), light-brown to brown, strong yellow-orange fluorescence particles to weak dark green fluorescence particles with fluorescence inclusions (acritarchs)	variable
			Homogeneous		
	Phytoclasts		Resin	Amber-coloured fragments, moderate orange fluorescence	20-40
STRUCTURED			Equidimensional opaque	Black particles with sharp angular outlines, no fluorescence	20-70
			Lath-shaped opaque		
			Fungal hyphae	Thin, branching ,tubular stuctures, absence or negligible fluorescence	variable
			Wood remains	Plant woody tissues (tracheids), light to dark brown particles with sharp angular edges and/or discernible cellular structure (pits &stripes)	30-80
			Cuticle remains	Epidermal fragments of leaves, roots, etc., pale yellow to light brown in color, weak to moderate fluorescence	15-50
			Degraded irregular plant cuticles	None apparent microstructure, irregular, angular, corroded outline, weak but clearly present fluorescence	
			Degraded plant tissue	Planar, irregular, angular, sharp cellular structures, yellow colour, moderate to strong green-yellow fluorescence	
	Terrestrial palynomorphs		Spores	Trilete spores with 3 laesurae (Y-mark), yellow colour with moderate orange fluorescence, *Lycopodium* is included	20-40
			Bisaccate pollen	Mostly, degraded and corroded exines with pyrite cepta, yellow, moderate orange fluorescence	10–30
			Non-bisaccate pollen		
	Aquatic palynomorphs	Marine algae	Acritarchs	Transparent single-celled organisms (algae), small size (≤5 µm), moderate size (5-10 µm) and large size (≥ 15 µm), large *Micrhystridium spp.* , colonial asseblages, strong yellow fluorescence	5–20
			Prasinophytes	*Tasmanites* & *Cymatiosphaera spp.*, strong yellow fluorescence	20-30
		Fresh water algae	Bortyococcus	Colonial structure(irregular globular colonies), lustrous colour, strong yellow fluorescence	20-40
		Zoomorphs	Foraminiferal test linings	Chitinous inner test of microforaminifera, planispiral, brown colour, weak but clearly present fluorescence	30-40
			Scolecodonts	Mouth parts of benthic polychaete annelid worms, brown colour, weak but clearly present fluorescence	30-40

3.6.1 Amorphous Group

Amorphous organic matter and resins as structureless products are classified in a more general Amorphous Group (Tyson, 1995).

Amorphous Organic Matter

Amorphous organic matter (AOM) has an either marine or terrestrial origin (Tyson, 1995). The marine AOM originates from organic aggregates of phytoplankton and/or zooplankton, faecal pellets, cyanobacteria and thiobacteria (Tyson, 1995).

Resin

Resin is natural product of higher plants which is derived either from internal cell or void filling secretions or extracellular exudations from the plant surfaces (Tyson, 1995). They are associated to coniferous gymnosperms of tropical and subtropical lowstand evergreen forest trees. The sediments deposited during Carnian Pluvial Event are plentiful in resins of millimeter size droplets (Breda et al., 2009).

3.6.2 Phytoclasts

Phytoclasts are classified in two main groups, the translucent and the opaque. They are remains and debris from higher plants (Tyson, 1995).

Translucent phytoclasts

The translucent phytoclasts are subdivided into wood remains, cuticle remains, degraded plant cuticles and plant tissues. The wood remains are derived from woody tissue from plants. They exhibit biostructures (Tyson, 1995). The cuticle remains and degraded plant cuticles are derived from leafs. They exhibit a cellular structure (Tyson, 1995). However, the plant tissues derive from the cellulose, non-woody part of plants and similar to cuticle remains exhibit cellular structure (Tyson, 1995).

Opaque phytoclasts

The oxidized or carbonized wood is defined as opaque phytoclast (Tyson, 1995). The term charcoal is used for wood products of forest fires or postdepositional processes. The opaques are subdivided in equidimensional (length:width < 3) and blade-shaped (length:width > 3) (Tyson, 1995).

3.6.3 Palynomorphs

The palynomorph group contains all organic microfossils. The organic microfossils can be of plant or animal affinity such as the sporomorphs, algae and zoomorphs.

Sporomorphs

Sporomorphs are the terrestrial palynomorphs such as spores and pollen. They are produced from embryophytes plants. Spores derived from bryophytes and ferns and pollen derived from gymnosperms and angiosperms (Traverse, 2007). Pollen and spores have different morphological characteristics. Spores are subdivided to monolete and trilete or alete depending on the number of laesurae, the scar "mark" form the contact between spores (Traverse, 2007). Pollen shows diversity in morphologies. The buoyancy of pollen is related to the air sacs. Bisaccate pollen is the most buoyant pollen. In the present study, the pollen is divided into bisaccate and non-bisaccate.

Acritarchs

Acritarchs are single-celled organisms of unknown biological affinity and show different morphologies (Traverse, 2007). They are either of algae origin or resting cysts of phytoplankton and indicate shallow water marginal marine facies. They can be found from brackish to hypersaline waters (Tyson, 1993).

Algae

Freshwater and marine algae such us *Botryococcus* and prasinophytes vary in size and shape. They are found in colonial structures or individually. These algae exhibit strong fluorescence (Tyson, 1995, Traverse, 2007).

Zoomorphs

Foraminiferal linings are chitinous inner test of microforaminifera (Traverse, 2007). They show an almost planispiral morphology. Scolecodonts are partly calcified and scleroproteinaceous mouth parts of benthic polychaete annelid worms (Tyson, 1995).

3.7 Interpretation techniques

3.7.1 Palynofacies kerogen parameters

Particular emphasis will be given to parameters that are used as indirect indicators for the palaeoenvironmental reconstruction. These are based in the classification and description of the kerogen constituents. There are many variables that are taken into consideration (Tyson, 1993), such as the biological origin of the particles as well as the ecology of different groups. Additionally, the preservation state and the morphological characteristics, the hydrocarbon generating potential and the degree of maturation are also significant. The parameters are summarized in Table 3.4.

Table 3.4: Palynofacies kerogen parameters used for palaeoenvironmental interpretation (modified after Tyson, 1995).

PARAMETER	SIGNIFICANCE OF HIGH VALUES
Opaque:other phytoclats ratio	Distal depositional environments, low TOC content indicate oxic conditions.
	Local high influx of charcoal due to wildfires and subsequently increase of runoff
	Postdepositional oxidation or local reworking from mature sediments, such as beaches, of phytoclasts
Equdimensional:lathshaped opaque phytoclast ratio	Low transportation distance. Proximal to fluvio-deltaic source
Marine:terrestrial palynomorph ratio	Indicate distal setting
Bisaccate:spores ratio	Depositional environment adjacent to land with conifers
	Low absolute abundance of bisaccates, distal depositional environments away from terrestrial sources or mainly aeolian transportation of sporomorphs
AOM fluorescence	High amount of fluorescence AOM indicate marine origin
Botryococcus	Fresh water indicator

3.7.2 AOM-phytoclast-palynomorph ternary diagram

The AOM-phytoclast-palynomorph (APP) plot has been used to characterize mainly the palaeoenvironment and secondly the kerogen assemblages (Fig.3.1)(Tyson, 1989, Tyson, 1993, Tyson, 1995). From the plot information about the proximity of the terrestrial organic matter source as well as for the redox status of the depositional subenvironments that are responsible for the preservation of AOM can be extracted (Tyson, 1993, Tyson, 1995).The interpretation of each palynofacies field is shown in Table 3.5.

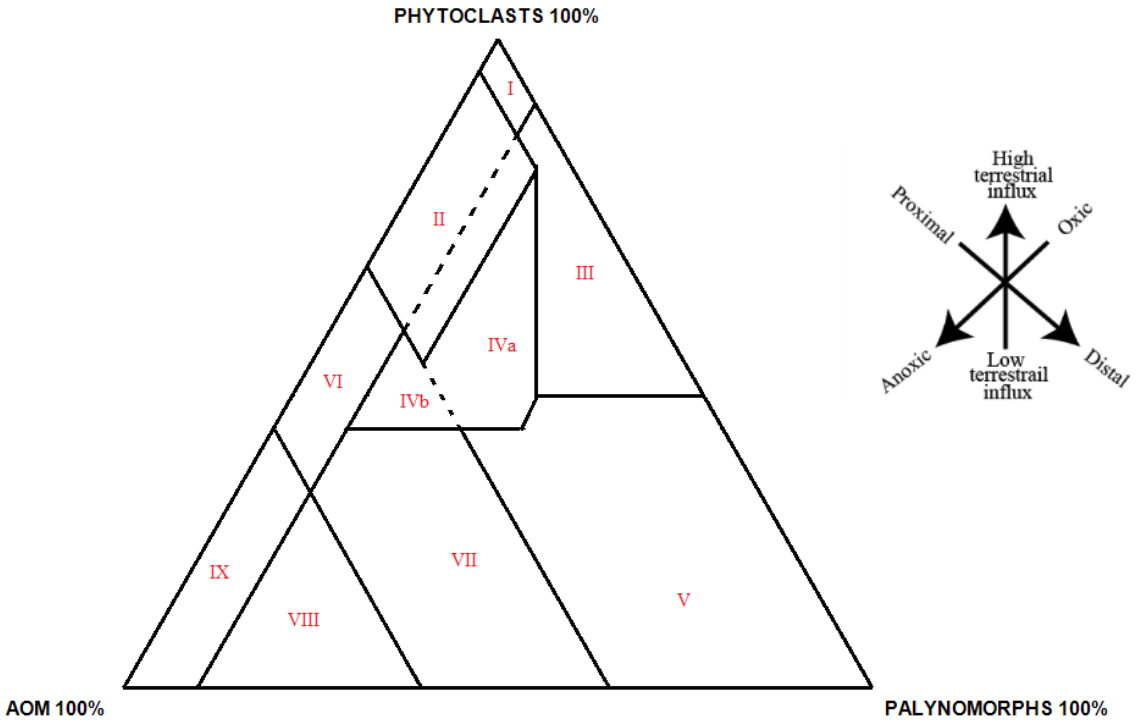

Fig. 3.1: The ternary APP- diagram. See Table 1 for field explanation (modified after Tyson, 1993).

Table 3.5: The environmental and kerogen type classification according to marine palynofacies (modified after Tyson, 1993).

Palynofacies field	Environment	Kerogen type
I	Highly proximal shelf or basin	III, gas prone
II	Marginal dysoxic-anoxic basin	III, gas prone
III	Heterolithic oxic shelf (’proximal shelf’)	III or IV, gas prone
IVa	Dysoxic-suboxic shelf or basin transition	III or II, mainly gas prone
IVb	Suboxic-anoxic shelf or basin transition	III or II, mainly gas prone
V	Mud-dominated oxic shelf (’distal shelf’)	III>IV, gas prone
VI	Proximal suboxic-anoxic shelf	II, oil prone
VII	Distal dysoxic-anoxic ’shelf’	II, oil prone
VIII	Distal dysoxic-anoxic shelf	II>>I, oil prone
IX	Distal suboxic-anoxic basin	II≥I, highly oil prone

3.7.3 Quality of organic matter

Geochemical data can be used as indicators of organic content qualitatively. The van Krevelen diagram of H/C versus O/C is the most classical tool for discriminating between the different types of kerogen (Fig. 3.2) (Tissot et al., 1974). There are four types of kerogen: type I which is very oil prone, type II which is oil prone, type III which is gas prone and type IV which consists of none prone inertinites.

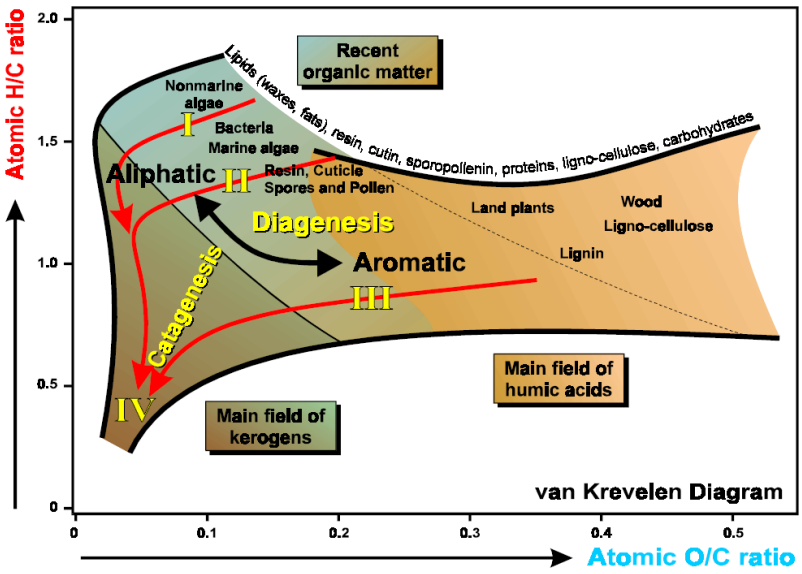

Figure 21, Atomic C, H, O composition of organic matter (modified from: Tissot & Welte, 1984).

Fig. 3.2: It shows the types of kerogen, using the atomic H/C versus O/C or the so called van Krevelen diagram (Tissot and Welte, 1984).

According to Espitalie et al. (1977), the carbon dioxide that is released during pyrolysis (S3) is equal to the amount of oxygen in the kerogen and the hydrocarbons that are released during pyrolysis (S2) are equal to the amount of hydrogen in the kerogen. They set the Hydrogen Index (HI) and Oxygen Index (OI) that are calculated as:

$$HI = \left(\frac{S2}{TOC}\right) \times 100 \quad \text{and} \quad OI = \left(\frac{S3}{TOC}\right) \times 100$$

Units of measurement is mg HC/g TOC and mg CO_2/g TOC, respectively. From the plot of HI versus OI the kerogen type (modified van Krevelen diagram) in the samples can be determined. Microscopic methods applied in the organic matter contribute to accurate results in addition to the geochemical data from pyrolysis.

In this interpretation, the data from Rock-Eval pyrolysis are used to classify the samples on the basis of the kerogen type. In particular, the S2/S3 ratio and HI are employed. After the kerogen type has been defined, it is easy to specify the main expelled products (oil, gas and none) at the peak of maturity of the organic matter. Peters and Cassa (1994) divide the HI, S2/S3 and atomic H/C into intervals (Table 3.6). Each interval is characterized by its unique kerogen type.

Table 3.6**:** Geochemical Parameters Describing Kerogen Type (Quality) and the Character of Expelled Products, modified after Peters and Cassa (1994).

Kerogen Type	HI (mg HC/g TOC)	S2/S3	Atomic H/C	Main expelled Product at Peak Maturity
I	>600	>15	>1.5	Oil
II	300-600	10.0-15.0	1.2-1.5	Oil
II/III	200-300	5.0-10.0	1.0-1.2	Mixed oil and gas
III	50-200	1.0-5.0	0.7-1.0	Gas
IV	<50	<1	<0.7	None

3.7.4 Quantity of organic matter

Petroleum potential or quantity of source rock is determined by the Total Organic Carbon (TOC) and the hydrocarbons that are released during pyrolysis –S2. According to Peters and Cassa (1994) , petroleum potential (quantity) is outlined by the organic matter of the source rock in terms of TOC, S1 and S2. It is, also, described by the amount of bitumen both in wt% and ppm, as well as from the amount of hydrocarbons in ppm (Table 3.7). Additionally, the genetic potential or petroleum potential represents the hydrocarbon generative potential. This index consists of the sum of the free released hydrocarbons (S1) and the hydrocarbons released during pyrolysis (S2). It is estimated by the function:

$$PP = S1 + S2 \ (mg\text{HC/g}TOC)$$

The data from Rock-Eval pyrolysis are examined under the criteria in Peters and Cassa (1994) in combination with the present diagram from Rock-Eval pyrolysis. The results are provided in Table 2. Additionally, the plot of S2 versus TOC is considerably useful in the determinations.

Table 3.7: Geochemical parameters describing the Petroleum Potential (Quantity) of an immature source rock, modified after Peters and Cassa (1994).

Petroleum Potential	TOC (wt%)	S1 (mg HC/g rock)	S2 (mg HC/g rock)	Bitumen (wt.%)	Bitumen (ppm)	Hydrocarbons (ppm)
Poor	0-0.5	0-0.5	0-2.5	0-0.05	0-500	0-300
Fair	0.5-1	0.5-1	2.5-5	0.05-0.10	500-1000	300-600
Good	1.0-2.0	1.0-2.0	5.0-10.0	0.10-0.20	1000-2000	600-1200
Very Good	2.0-4.0	2.0-4.0	10.0-20.0	0.20-0.40	2000-4000	1200-2400
Excellent	>4	>4	>20	>0.40	>4000	>2400

3.7.5 Thermal maturity of organic matter

There are three main stages of maturation according to thermal evolution: diagenesis (immature), catagenesis (mature) and metagenesis (postmature). There are some indices that are used in the evaluation of hydrocarbons in terms of maturity. The Production Index (PI) which is calculated as below:

$$PI = \frac{S1}{[S1 + S2]}$$

This ratio represents the generated hydrocarbons to petroleum potential. It is used to define the evolution level of the organic matter. The oil window corresponds to the interval of values between 0.08-0.4. Additionally, another important parameter is the T_{max} (°C), which is the temperature of maximum release of hydrocarbons (S2).

Peters and Cassa (1994) set some evaluation criteria for the thermal maturation of source rocks (Table1). For the assessment of the maturity level, they mainly used vitrinite

reflectance Ro (%), Tmax (°C) and the Thermal Alteration Index (TAI). Ro and TAI are organic petrological techniques. Other parameters use the amount of generated hydrocarbons in order to define the thermal maturity. These indices are Bitumen (mg/g EOM-extractable organic matter), Bitumen/TOC the Production Index.

The Thermal Alteration Index is an indication colour of pollen and spores on a reference scale (Staplin, 1982). The slides from the sample are examined under the transmitted light microscope. The colour of the spores and pollen is identified in accordance with TAI scales. This method is subjective because it partly depends on the interpretation of the microscopist.

Vitrinite Reflectance (Ro) indicates the level of thermal maturity of the percentage of the reflected incident light from vitrinite particles in the sample (Espitalié, 1986). There are minimum and maximum values of vitrinite reflectance. The oil window is defined to be between Ro=0.5% and Ro=1.3%.

Table 3.8: Geochemical Parameters Describing Level of Thermal Maturation, modified after Peters and Cassa (1994).

Stage of Thermal Maturity for Oil	Ro(%)	Tmax(°C)	TAI	Bitumen/ TOC	Bitumen (mg/g rock)	PI [S1/(S1+S2)]
Immature	**0.2-0.6**	**<435**	**1.5-2.6**	**<0.05**	**<50**	**<0.10**
Mature						
Early	**0.6-0.65**	**435-446**	**2.6-2.7**	**0.05-0.10**	**50-100**	**0.10-0.15**
Peak	**0.65-0.9**	**445-450**	**2.7-2.9**	**0.15-0.25**	**150-250**	**0.25-0.40**
Late	**0.9-1.35**	**450-470**	**2.9-3.3**			**>0.40**
Postmature	**>1.35**	**>470**	**>3.3**			

4. Results

4.1 Palynofacies

The particulate organic matter (POM) of each slide has been determined. The number of countings per slides ranges from 266- 483 (avg. 355). Their classification is on the relative frequencies of the three categories of palynological matter: palynomorphs, phytoclasts (translucent and opaque) and AOM. Characteristic palynomorphs are depicted on Plate 1, whereas the distribution of components of the palynological matter is shown in Figure 4.1.

Throughout the studied section the amorphous organic matter is dominate the total sum of the total particulate organic matter (TPOM), except for slides SBG2 41,SBG2 42, SBG2 44 where cuticles are dominating and STB5, STB8 where the wood remains are abundant. Phytoclasts have a significant presence in the TPOM. Equidimensional and lath- shaped opaques ranging between 0.4% and 20% (avg. 6%) and between 0.2% and 5% (avg. 1.3%) of TPOM, respectively. Woody remains are abundant with 3%-46% (avg. 12%). The cuticle remains, degraded plant cuticles and plant tissues are fluctuating between 0.2%-6.0% (avg. 10%) of TPOM. Additionally, clusters of pyrite and pyritization of TPOM were present in all samples.

The relative abundances of palynomorphs range, to a large extent, in the assemblages throughout the study section, spanning between 0.2%-24% (avg. 21%). The continental palynomorphs are the dominant group with up to 24% (avg. 18%) of TPOM. Pollens are the greatest contributors with 1.2% -24% (avg. 11%), closely followed by bissacate pollens (avg. 5%). Spores vary between 0.2%-13 % (avg. 2%). Lastly, freshwater algae Botryococcus reaches up to 0.7%. The relative abundance of marine palynomorphs are between 0.2%-8% (avg. 3%) of TPOM. Acritarchs of Micrhystridium spp. and other algae remains are significant contributors and range between 0.2%-8% (avg. 3%) and Tasmanites and Cymatiosphaera spp. (prasinophytes) between 0.3%-1.5% (avg. 0.4%). Within the marine group the foraminiferal test linings are ranging between 0.5%-1% (avg. 0.2%) and scolecodonts up to 0.2% of TPOM.

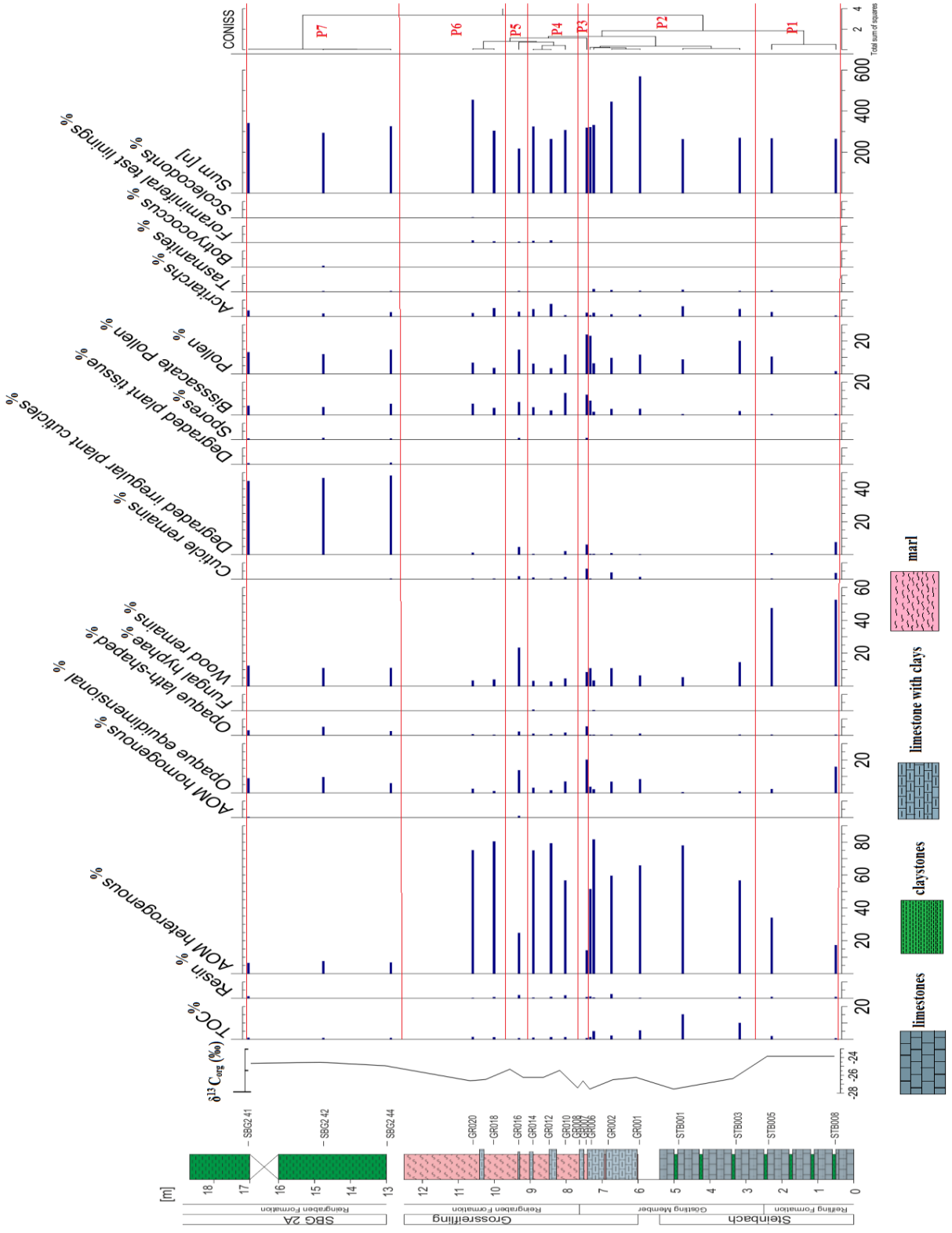

Fig. 4.1: The relative abundances in relation with the TOC, δ13Corg and lithology. It is shown, also, the classification in palynofacies zones.

From the amorphous group, amorphous organic matter (AOM) is fluctuating in relative abundance, ranging from 0.2% to 81% of TPOM (avg. 48%). In the fluorescent light analysis most of the AOM reacted highly to the exposure to fluorescent light. Lastly, resin varies between 0.2%-3% (avg. 0.7%).

The samples were classified into seven main clusters of distinct palynofacies assemblage zones, denoted as P1, P2, P3, P4, P5, P6, P7 (Fig. 4.1). Assemblage zones using cluster analysis (CONISS) with Tilia were established.

Additionally, the samples are plotted in the APP ternary diagram in order to categorize them in different marine palynofacies fields (Fig 4.2). Five palynofacies fields are defined, while palaeoenvironmental and kerogen type assumptions have been carried out for each palynofacies field (Table 4.1), according to Tyson (1993).

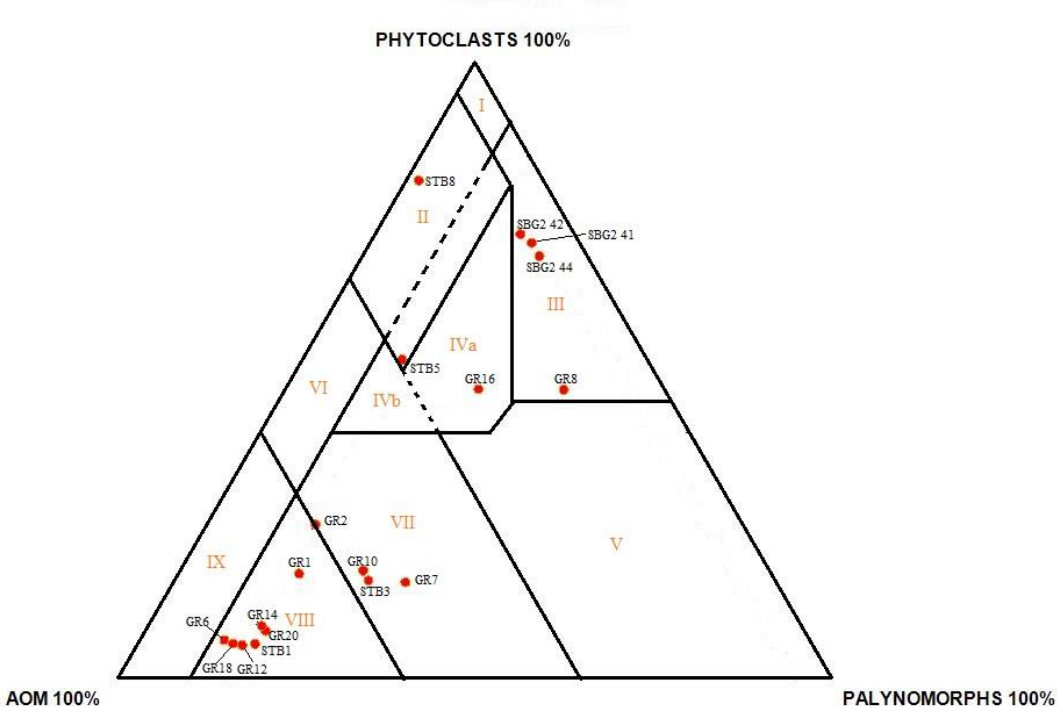

Fig. 4.2: The ternary APP diagram and the plotted samples. The samples are distributed in different marine palynofacies fields. In addition, the green circle represents the phytoclasts dominating samples, whereas the red circle indicates the AOM dominating samples.

Table 4.1: The interpretation of each sample in terms of palynofacies, environment and kerogen type.

Palynofacies field	Environment	Kerogen type	Interpretation of samples
II	Marginal dysoxic-anoxic basin	III, gas prone	STB8, STB5
III	Heterolithic oxic shelf ('proximal shelf')	III or IV, gas prone	GR8, SBG2 41, SBG2 42, SBG2 44
IVa	Dysoxic-suboxic shelf or basin transition	III or II, mainly gas prone	GR16
VII	Distal dysoxic-anoxic 'shelf'	II, oil prone	GR2, GR7, GR10, STB3
VIII	Distal dysoxic-anoxic shelf	II>>I, oil prone	GR1, GR6, GR12, GR14, GR18, GR20, STB1

It is observed that samples can be separated in two main groups. The first group is dominating by phytoclasts over the three fifths of the total POM and consists of samples: STB8, GR8, SBG2 41, SBG2 42, SBG2 44, STB5, and GR16. The second group is occupied by AOM over the half of total POM and contains the samples: GR1, GR2, GR6, GR7, GR10, GR12, GR14, GR18, GR20, STB1, and STB3.

In phytoclasts dominated part are indicated by palynofacies fields II, III, IVa. Palynofacies field II is represented by sample STB8. It is interpreted as marginal dysoxic to anoxic basin and reveals kerogen type III which is gas prone. Additionally, palynofacies field III contains the samples GR8, SBG2 41, SBG2 42, and SBG2 44 and describes a heterolithic oxic shelf environment which is in the proximal shelf, while the kerogen type is III or IV revealing mostly gas potential. Last but not least, palynofacies field IVa includes the samples STB5, GR16. This palynofacies corresponds to dysoxic -suboxic shelf or the basin transition and coincides with mainly gas prone kerogen of type III or II.

The palynofacies fields VII and VIII are AOM dominated. Both of them indicate distal dysoxic to anoxic shelf with the kerogen characterizing mainly as type II of oil prone. Palynofacies VII includes the samples GR2, GR7, GR10, STB3, while palynofacies field VIII contains the samples GR1, GR6, GR12, GR14, GR18, GR20, and STB1.

Palynofacies zones from the cluster analysis combined with the environmental interpretation from Tyson (1993) shows that high abundances of phytoclasts and sporomorphs coincide with oxic-suboxic environments (Fig. 4.4). However, the high abundances of AOM and algae coincide with dysoxic-anoxic environments (Fig. 4.4).

Lastly, the interpretation of the palynofacies kerogen parameters of Tyson (1995) indicates a general trend of proximity to the fluvio-deltaic source (Fig. 4.3). Palynofacies 3, 5 and 7 show a more terrestrial influence having the lowest marine: terrestrial palynomorphs ratio.

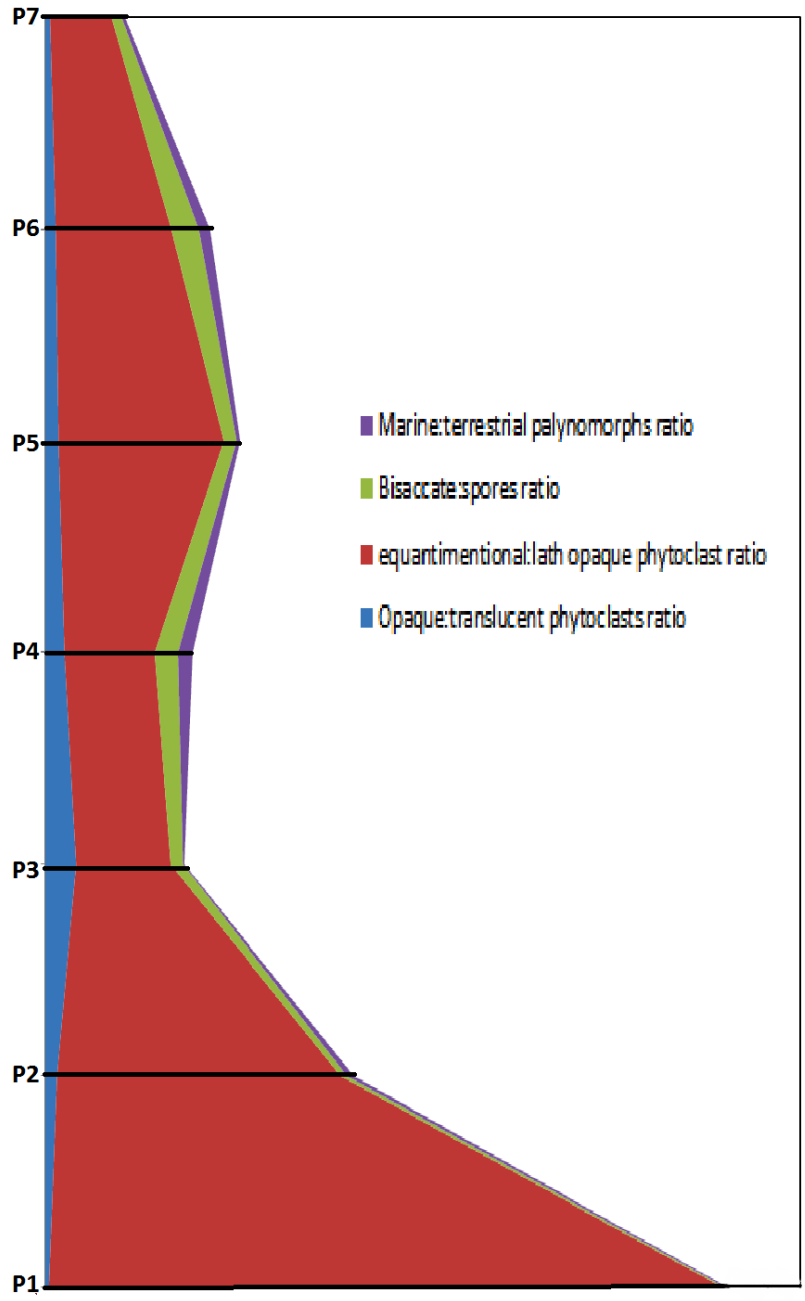

Fig. 4.3: The palynofacies kerogen parameters show a proximal trend to the fluvio-deltaic source

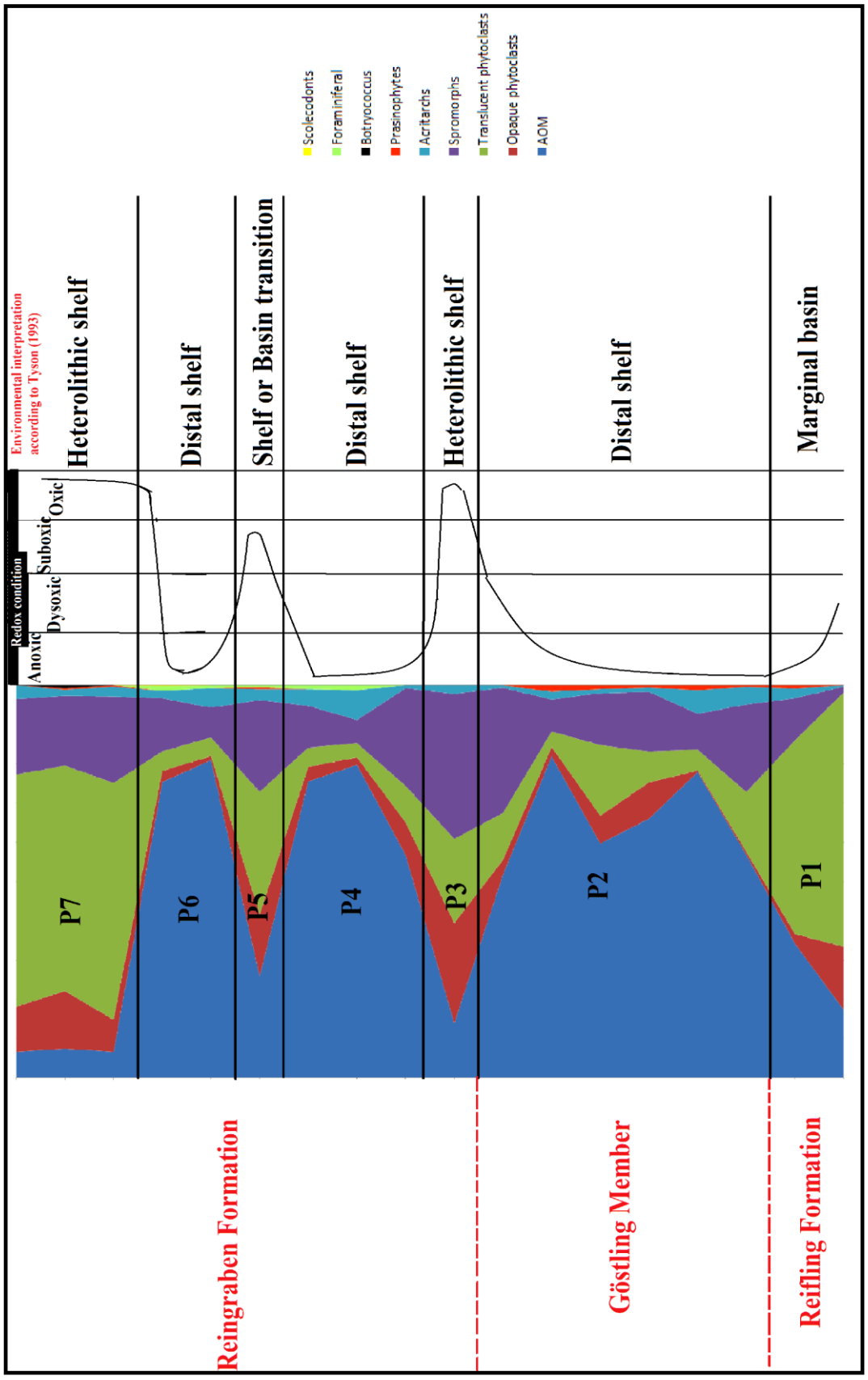

Fig. 4.4: Palynofacies and its redox environments throughout Reifling Formation, Göstling Member and Reingraben Formation.

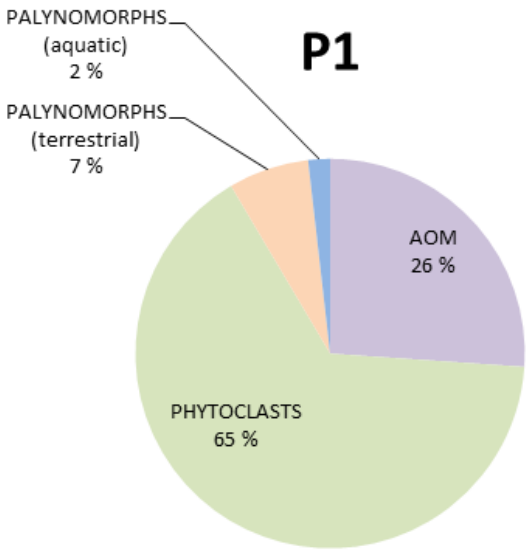

4.2 Palynofacies zones

Palynofacies zone 1 (439.3-437.4 m) (P1)

Sample: STB5 & STB8

Section: Steinbach

Lithological unit: Reifling Formation

The basal palynofacies zone is dominated by terrestrially-derived organic matter, with an overall dominance of phytoclasts of a high average relative abundance, especially wood remains (avg. 50%), while the terrestrial palynomorphs have a very low average relative abundance of 7%. The equidimensional opaque phytoclasts show a decreasing trend through the palynofacies. The cuticle remains (avg. 2%) and degraded irregular cuticles (avg. 4%) decrease upward. The upper boundary is marked by an increase of AOM and pollen reaching 34% and 10%, respectively (Fig. 4.4). Aquatic palynomorphs are the minority with only consisting mainly from acritarchs of *Micrhystridium* spp. and prasinophytes of type *Tasmanites*.

The organic $\delta^{13}C_{org}$ content is stable around -23.6‰ to -23.7‰ (Fig.1). The TOC content increases towards the upper boundary, beginning with 0,61wt% and rise to 1,9wt% (Fig.4.1).

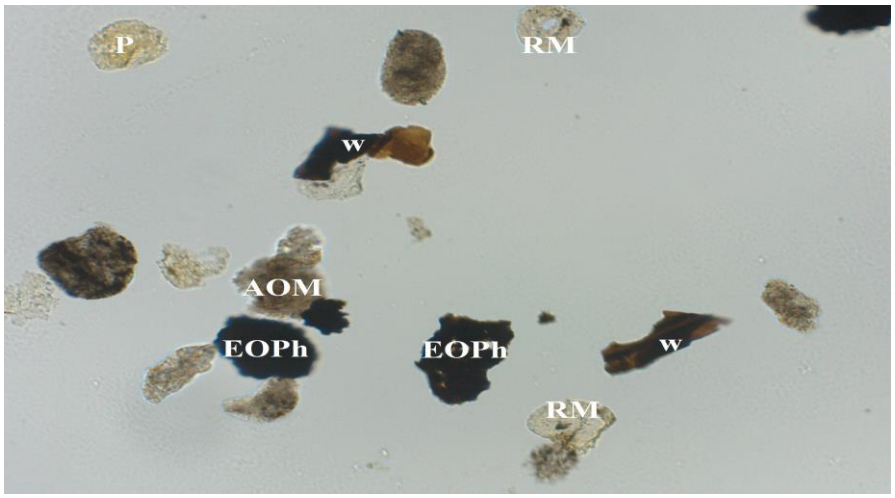

Fig. 4.5: The **palynofacies-type 1**, sample STB5, **P**: pollen, **EOPh**: equidimensional opaque phytoclast, **W**: wood remains, **AOM**: amorphous organic matter, **RM**: residual mineral.

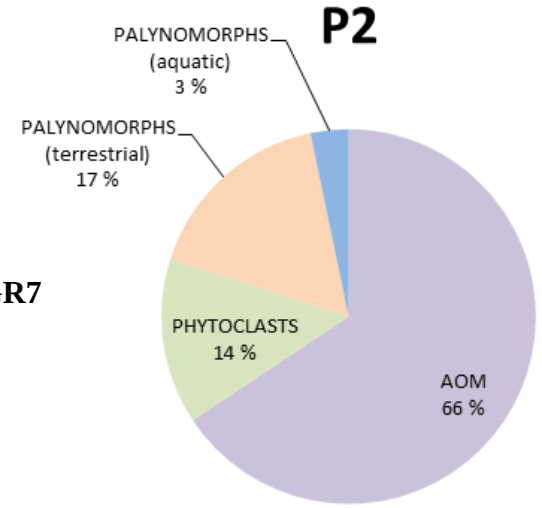

Palynofacies zone 2 (436.4-431.5 m) (P2)

Sample: STB3, STB1, GR1, GR2, GR6 & GR7

Section: Steinbach & Grossreifling

Lithological unit: Göstling Member

The second palynofacies zone is characterized by the onset of CPE. The amount of AOM is high. However, AOM fluctuates and reaches a peak of 82% just about the upper boundary. Terrestrial palynomorphs are the second high assemblage with a moderate relative abundance consisting particularly from pollen (avg. 13%) and bisaccate pollen (avg. 3%) (*Ovalipollis* spp., *Triadispora* spp.) Wood remains decrease significantly compared to palynofacies zone 1, reaching an average relative abundance of 8.4%. Generally, both wood remains and pollen show high abundances in the lower and upper part of the palynofacies zone, exceptionally another peak of woods is up from the middle part of the zone. These peaks coincide with the lowest abundances of AOM. Cuticles are almost absent except the peak of 4% that presents up from the middle part of the zone. Noticeably, equidimensional opaque phytoclasts show a sharply increasing trend. Acritarchs have a decreasing trend that starts with approximately 6% and ends with 0.7% in the upper part of the zone, whereas prasinophytes of the type of *Cymatiosphaera* spp. and *Tasmanites* remain almost constant.

The positive trend of $\delta^{13} C_{org}$ is suddenly interrupted at the boundary of Reifling Fm. and Göstling Member., as the $\delta^{13} C_{org}$ shifts towards more negative values, with a 3-4‰ negative difference. The carbon isotope values remain depressed throughout most of the thin-bedded clay-rich limestones and the shales of Göstling Member and Reingraben Formation.

TOC shows a sudden increase of values with a high range from 1-15%. In the base of the palynofacies zone, the abrupt change is estimated as 5% continuing with high values and reaches the maximum of 15%. However, after this peak, it is observed a decreasing trend (Fig. 4.1).

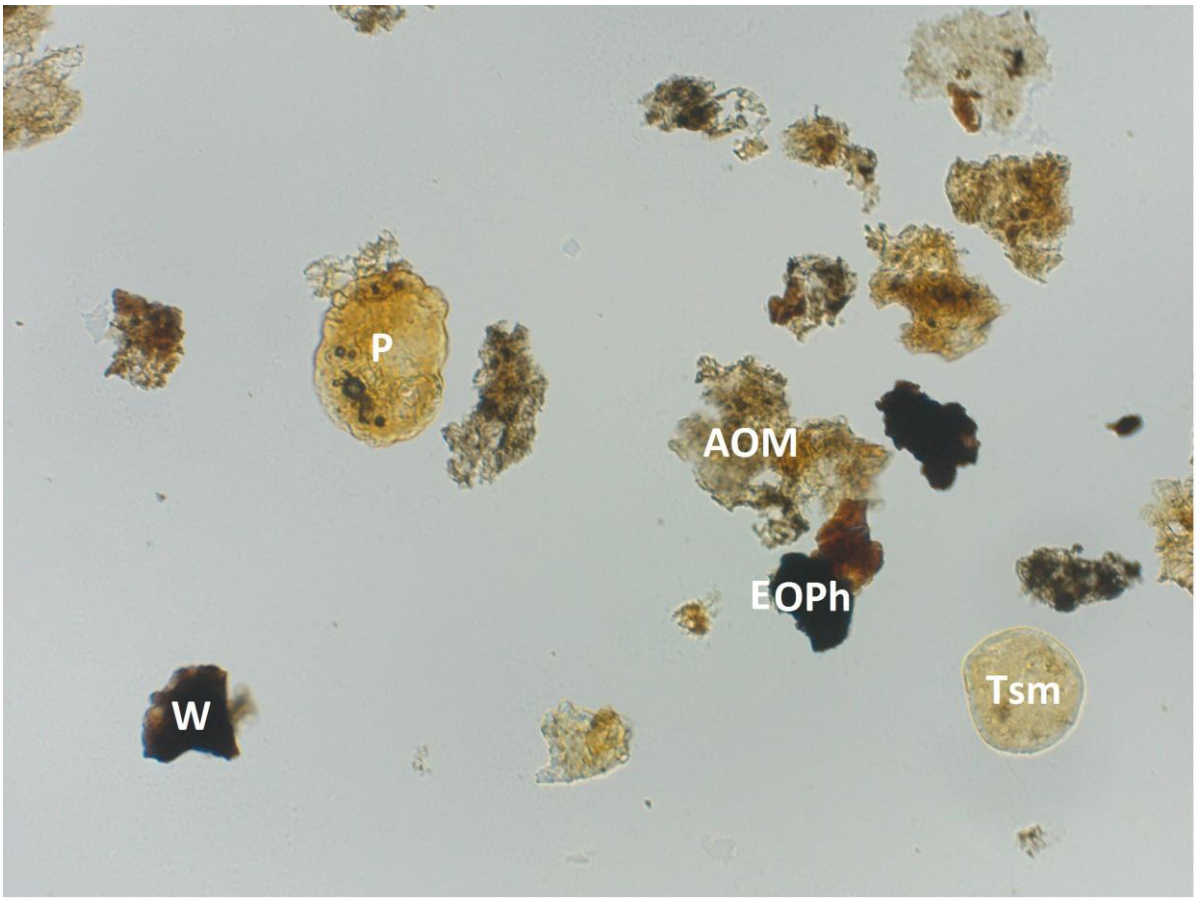

Fig. 4.6: The **palynofacies-type 2**, sample GR2, **P**: pollen, **EOPh**: equidimensional opaque phytoclast, **W**: wood remains, **Tsm**: Tasmanites, **AOM**: amorhous organic matter.

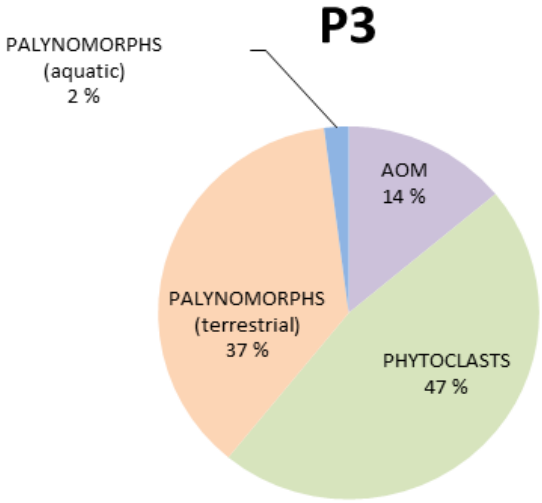

Palynofacies zone 3 (431.2 m) (P3)

Sample: GR8

Section: Grossreifling

Lithological unit: Reingraben Fm

The third palynofacies zone is dominated by almost the half from phytoclasts, with the bulk occupied by equidimensional opaque phytoclasts (avg. 20%). However, significant increase is shown by cuticles (remains and degraded) (avg. 12%), woods (avg. 9%). Lath-shaped opaque phytoclasts show an abrupt increase compare to palynofacies zone 2 reaching an average abundance of 5%. The two fifth are occupied by terrestrial palynomorphs containing pollen (avg. 24%) and bisaccates (avg. 12%) (e.g. *Enzonalasporites vigens* and *Partitisporites* spp.). Additionally, trilete spores are observed in a low relative abundance of the type *Aratrisporites* spp. In comparison to palynofacies 2, AOM decreases abruptly by half (avg. 14%). However, acritarchs of *Micrhystridium* spp. are quite stable, but prasinophytes of type *Tasmanites* is absent.

Throughout the palynofacies zone, $\delta^{13}C_{org}$ displays a negative excursion of -27‰ and low TOC (0.7%) (Fig. 4.1).

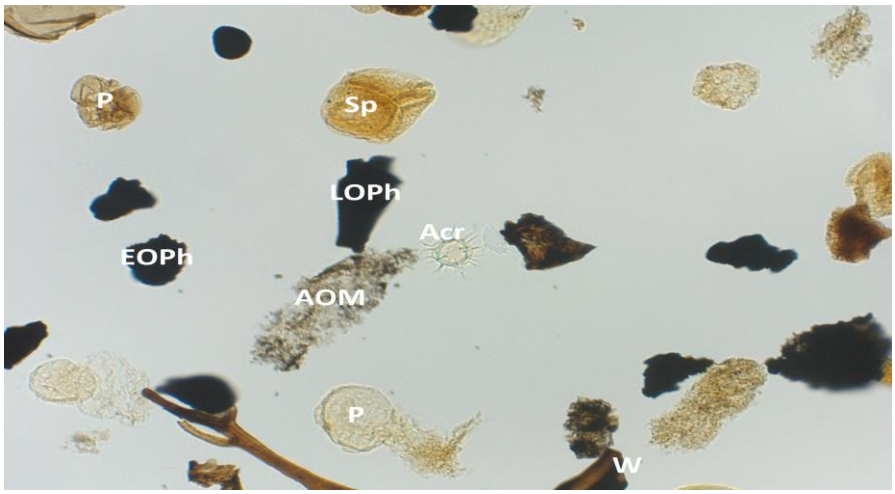

Fig. 4.7: The **palynofacies-type 3**, sample GR5, **P**: pollen, **Sp**: spore, **Acr**: acritarch, **LOPh**: lath-shaped opaque phytoclast, **EOPh**: equidimensional opaque phytoclast, **AOM**: amorphous organic matter, **W**: wood remain.

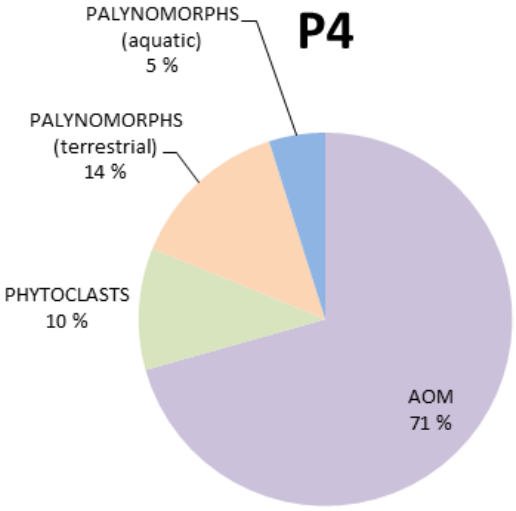

Palynofacies zone 4 (430.8-429.8 m) (P4)

Sample: GR10, GR12 &GR14

Section: Grossreifling

Lithological unit: Reingraben Formation

Palynofacies zone 4 is dominated by AOM with a high relative abundance which coincides with the highest relative abundance of acritarch (avg. 4%) compared to the other six palynofacies. In the base of the palynofacies zone the bisaccate pollens (e.g. *Lunatisporites acutus* spp.) and pollens (e.g. *Aulisporites astigmosus, Cycadopites* spp.) show significally equal low relative abundances (avg. 7% each) in comparison to phytoclasts (avg. 10%) where the most representative groups are equidimensional opaque phytoclast (avg. 4%) and wood remains (avg. 3%). Upwards, both terrestrial palynomorphs and opaque and wood phytoclasts follow a slightly decreasing trend. Exceptionally, very low relative abundances of cuticles remains are stable, while degraded forms are disappearing upwards. The palynofacies is characterized by the absent of spores.

After a negative excursion in palynofacies 3, the $\delta^{13}C_{org}$ content rises slightly by 1-2‰ and gets stable at about -26‰. The TOC content characterizes by a decreasing trend from 1.3% to 0.9% (Fig. 4.1).

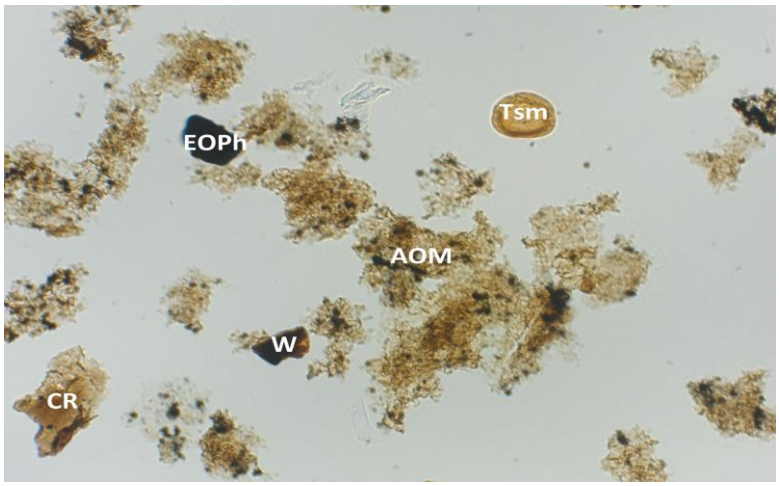

Fig. 4.8: The **palynofacies-type 4**, sample GR12, **AOM**: amorphous organic matter, **Tsm**: Tasmanites, **W**: wood remain, **EOPh**: equidimensional opaque phytoclast, **CR**: cuticle remain.

Palynofacies zone 5 (429.4 m) (P5)

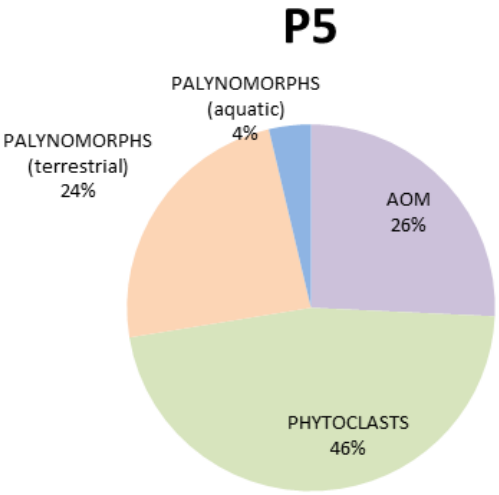

Sample: GR16

Section: Grossreifling

Lithological unit: Reingraben Formation

Palynofacies 5 shows a similarity to palynofacies 3, which is related to the abrupt decrease of AOM and sharp increase of terrigenous components such as phytoclasts and terrestrial palynomorphs keeping the three quarter of the palynofacies zone. The most abundant group of phytoclasts are wood remains with a moderate relative abundance and, secondly, the opaque equidimensional phytoclasts of even lower relative abundance, while lath-shaped opaque phytoclasts, cuticle remains and degraded irregular cuticles are minority. On the other hand, the terrestrial group is dominated mostly by pollen (15%) of *Aulisporites astigmosus*, *Cycadopites* spp. and less of bisaccate pollen (8%). Spores have a relative abundance of 1%. The aquatic palynomorphs consist from acritarch of *Micrhystridium* spp (3%), prasinophytes of the types *Cymatiosphaera* spp. and *Tasmanites* and foraminiferal test linings.

A positive excursion of δ^{13} C_{org} is slightly high than the previous palynofacies about -25‰. The TOC value is low about 0.7% (Fig. 4.1).

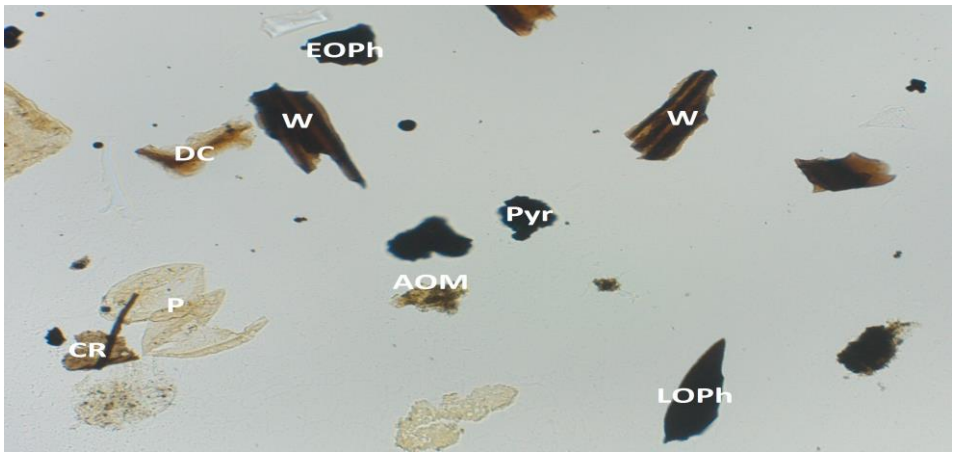

Fig. 4.9: The **palynofacies-type 5**, sample GR16, **P**: pollen, **LOPh**: lath-shaped opaque phytoclast, **EOPh**: equidimensional opaque phytoclast, **AOM**: amorphous organic matter, **W**: wood remain, **CR**: cuticle remain, **DC**: degraded cuticle, **Pyr**: pyrite.

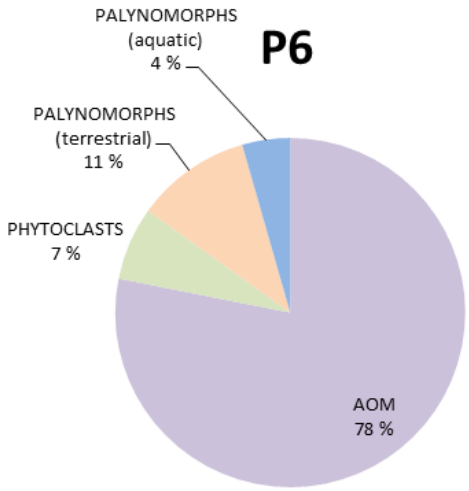

Palynofacies zone 6 (428.8- 428.4 m) (P6)

Sample: GR18 & GR20

Section: Grossreifling

Lithological unit: Reingraben Formation

Palynofacies 6 is dominated by AOM with a high relative abundance of the three quarter of the total zone. The rest components are mainly low terrestrial palynomorphs abundance containing almost equal relative abundances of bisaccates and pollens (e.g. *Aulisporites astigmosus*, *Cycadopites* spp.). The aquatic palynomorphs consist from acritarch of Micrhystridium spp (avg. 3%), foraminiferal test linings (avg. 1%) and scolecodonts (avg. 0.1%). Phytoclasts have the lowest relative abundance of all palynofacies including mainly wood remains, equidimensional opaque phytoclasts, lath-shaped opaque phytoclasts, cuticle remains (avg. 0.4%) and degraded irregular cuticles (avg. 1%).

After the positive excursion of palynofacies 5, the $\delta^{13}C_{org}$ content falls slightly about 1‰. The TOC values remain almost the same (Fig. 4.1).

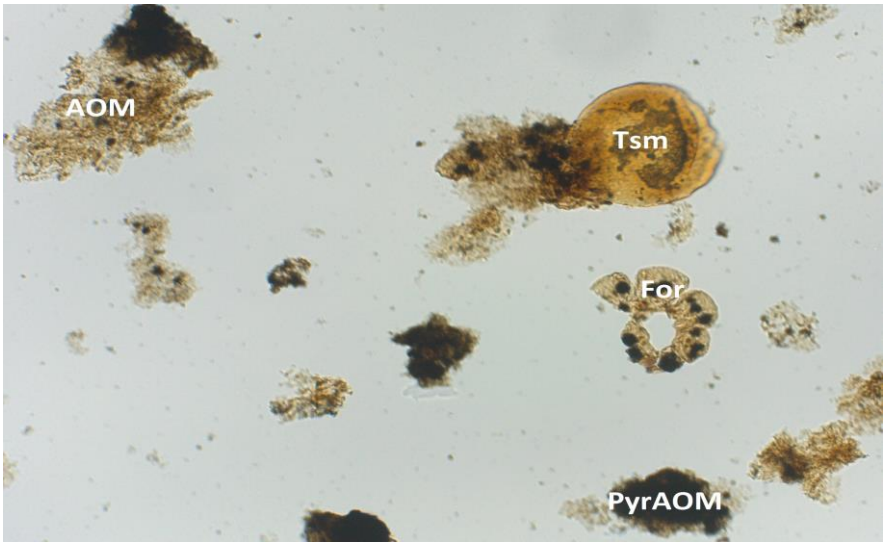

Fig. 4.10: The **palynofacies-type 6**, sample GR20, **AOM**: amorphous organic matter, **PyrAOM**: Pyritization of AOM, **Tsm**: Tasmanites, **For**: Foraminiferal test linings.

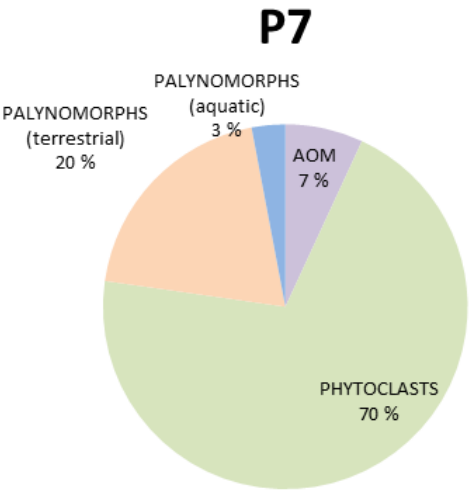

Palynofacies zone 7 (419-415 m) (P7)

Sample: SBG2 41, SBG2 42, SBG2 44

Section: Sulzbachgraben-2

Lithological unit: Reingraben Formation

The topmost palynofacies 7 is dominated by terrestrial-derived organic matter, with high concetration of phytoclasts including the half of degraded irregular cuticles. However, opaque phytoclasts and wood remains are low. Degraded plant tissues are found in the lower and upper part of the palynofacies. However, AOM is extremely low if compared with the rest palynofacies with a relative abundance of 7%. Sporomorphs are almost stable throughout the interval and have low relative abundance consisting of pollen (avg. 13%) (e.g. *Aulisporites astigmosus*, *Cycadopites* spp.), bisaccates (avg. 6%) and spores (avg. 1%). *Botryococcus* is observed in the middle part of this interval with a extremely low relative abunance (avg. 0.2%), as well as prasinophytes of the type *Tasmanites*. Nevertheless, acritarch of *Micrhystridium* spp. (avg. 3%) are almost equally distributed throughout the interval.

A continuous positive trend of $\delta^{13}C_{org}$ is observed that rises up slightly from -24.7‰ to -24.5‰. However, TOC values fluctuate around 0.83% (Fig. 4.1).

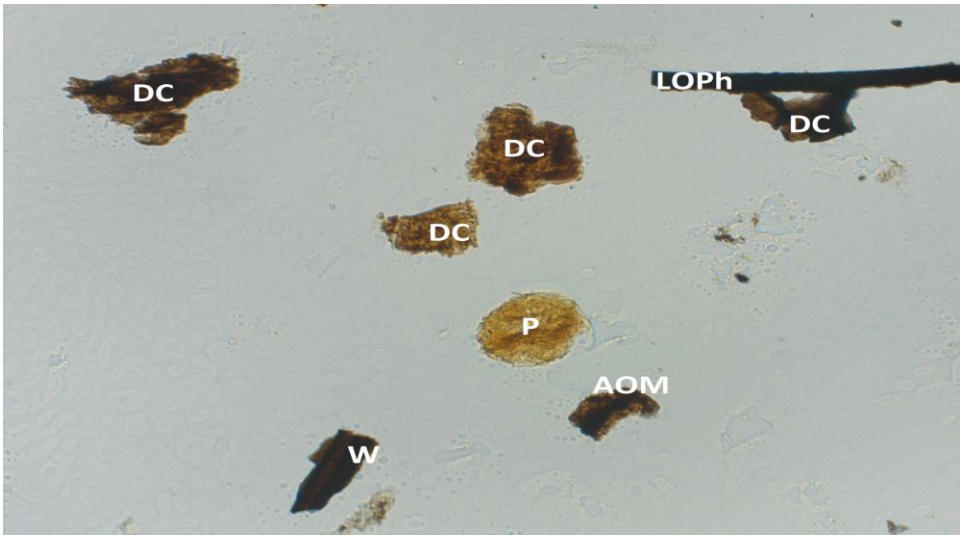

Fig. 4.11: The **palynofacies-type 7**, sample SBG2 42, **AOM**: amorphous organic matter, **DC**: degraded cuticle, **P**: pollen, **W**: wood remain, **LOPh**: lath-shaped opaque phytoclast.

4.3 The paradox of acritarchs

In the present study acritarchs are of particular interest due to the different sizes distinguishing them to small size (≤5 μm), moderate size (5-10 μm) and large size (≥ 15 μm) (Fig. 4.12). These observations have been carried out using the UV light microscope. Small and moderate acritarchs are found in AOM as inclusions, while the large acanthomorph acritarchs of *Micrhystridium* "complex" are found as individual particles or assemblages. Figure 4.12 shows the distribution of the different sizes of acritarchs compared to the AOM. They were selected representatives sample of high, moderate and low AOM. It is perceived that the samples with high AOM that ranges between 75%-81% of the total POM contain abundant small acritarchs occupying about 80% and in a less extent moderate size acritarchs holding the rest 20% (Fig. 4.13). However, the samples with moderate AOM of 51-70% contain approximately 72% of small acritarchs, 26% moderate acritarchs and 2% of large acritarchs. Lastly, the sample with low AOM of 25% consists mainly from 84% small acritarchs and 16% moderate size acritarch.

Possible explainations of the small size acritarchs are given by Tyson (1993) and it is due to the sieving that has been used during sample preparation and thus the acritarchs are tiny fragments and/or they are whole bodies of acritarchs that covered by AOM and thus are overlooked.

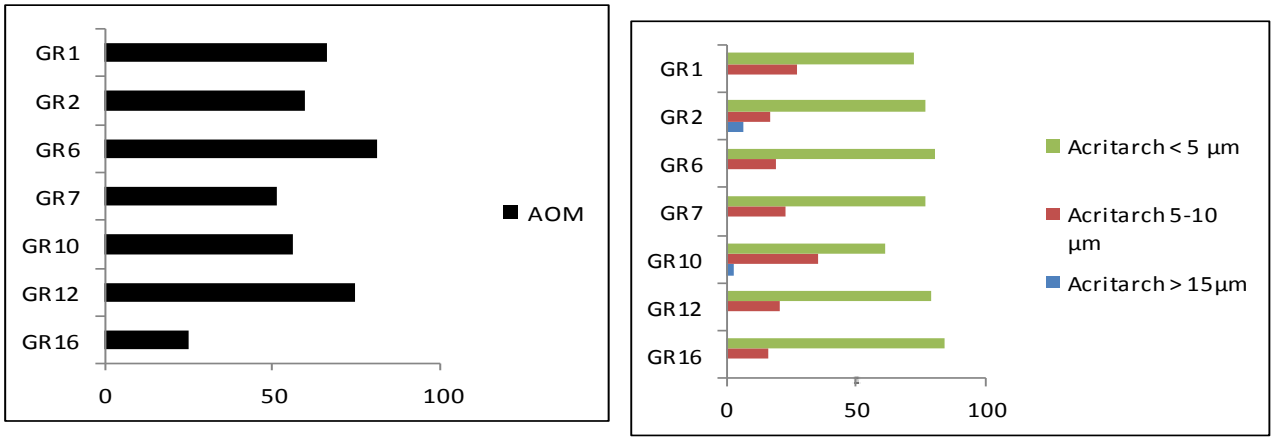

Fig.4.12 : The diagrams show the varied size of acritarchs and their distribution among the AOM. The samples GR6, GR12 have high AOM, GR1, GR2, GR7, GR10 have moderate AOM and GR16 have low AOM.

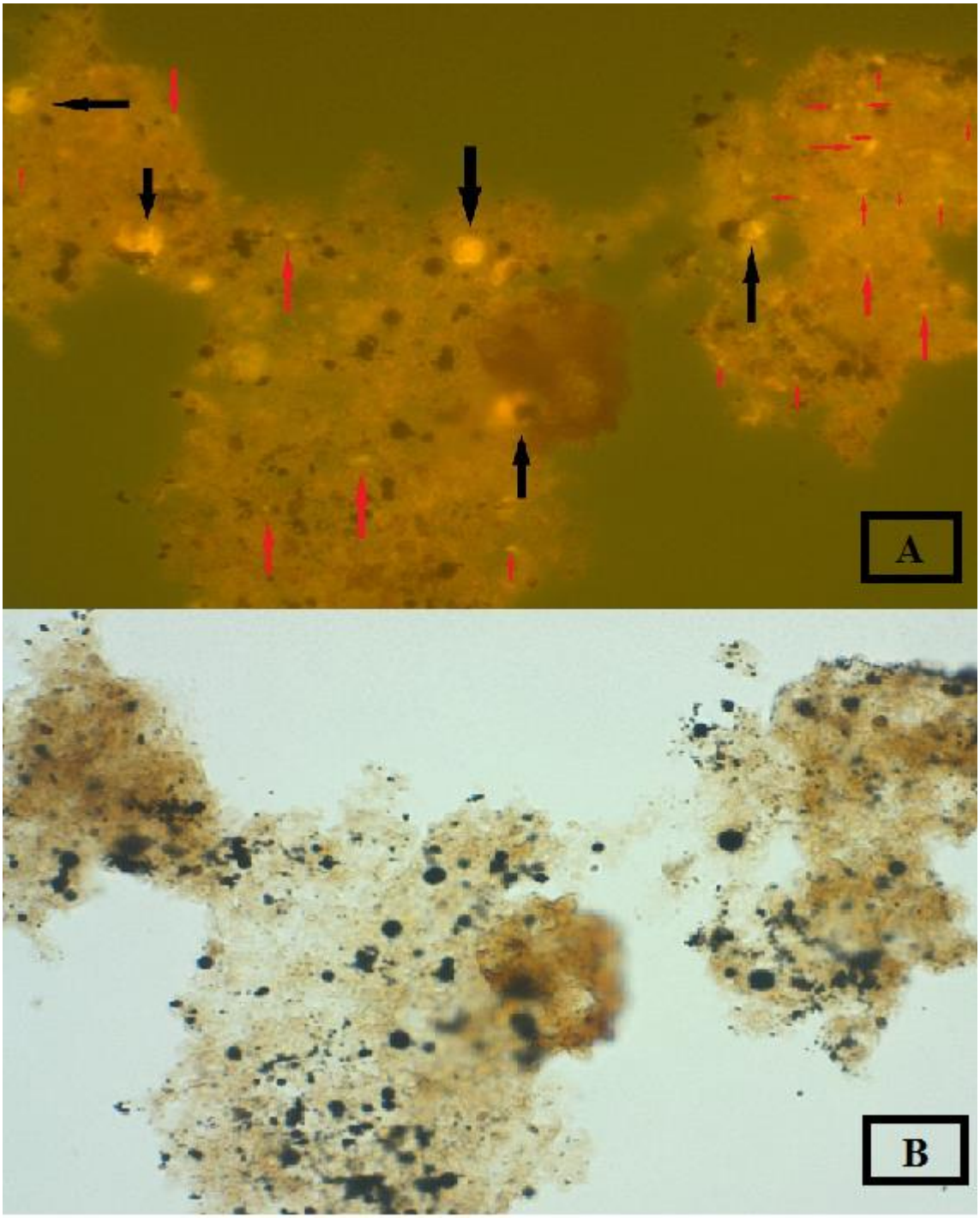

Fig. 4.13: Samlpe with high abundance of AOM (Sample GR12). A. AOM under fluorescence UV light and the distribution of small and moderate size acritarchs. The black arrows indicate the moderate size acritarch (5-10 µm) and the red arrows the small size acritarchs (≤5 µm). B. Under transmitted light the acritarchs are difficult to recognized (Tyson, 1995).

4.4 Geochemical interpretation

4.4.1 Quality of organic matter

In Table 4.2 the results of the Rock- Eval pyrolysis are displayed, simultaneously taking into consideration the criteria from Peters and Cassa (1994). GR1 and STB1 samples have the best oil and gas prone kerogen type compared to others. GR1 and STB1 have type II/III kerogen which can expel mixed oil and gas. The standard deviation for the HI parameter is approximately 10 for our internal standard, which has a TOC of approximately 3%. Therefore a HI of 201 (GR1) could also be 190 or 210 (Peters, 1986). Samples which highlighted with green colour are characterized by kerogen type III which can expel some amount of gas. A slightly possibility of expulsion of gas from samples that highlighted with pink colour and they indicated by an intermediate character between type III and type IV. The rest samples are described as type IV kerogen and contain "dead carbon". Additionally, the modified Van Krevelen of HI versus OI diagram shows almost the same results (Fig. 4.14). The boundary of HI equal to 50 mg HC/g TOC has been used for distinguishing between kerogen types III and IV.

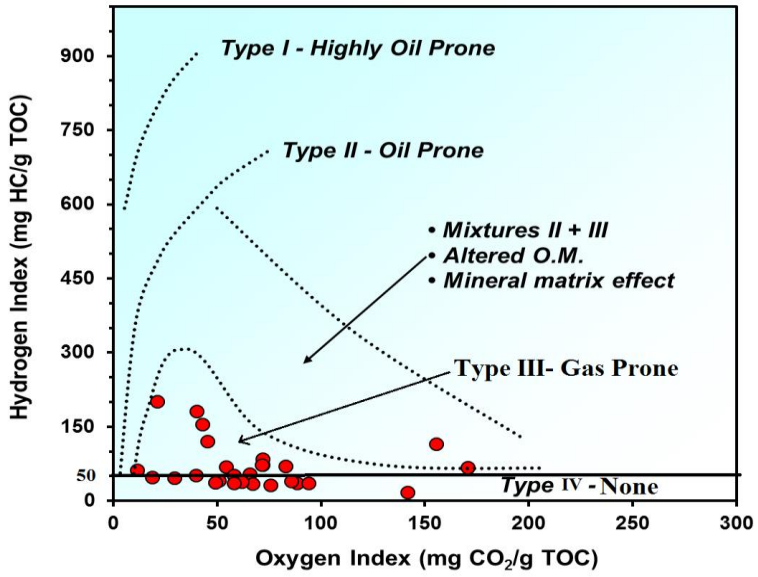

Fig. 4.14: The diagram of Hydrogen Index (HI) versus Oxygen Index (OI) that defines the types of kerogen.

Table 4.2: The interpreted samples in terms of kerogen type and associated expelled products.

Sample	Depth (m)	S2/S3	HI (mg HC/g TOC)	Kerogen Type	Main expelled Product at Peak Maturity
GR1	432.9	9.50	201	II/III	Mixed oil and gas
GR2	432.2	0.84	70	III-IV	Gas to None
GR6	431.7	2.52	47	III-IV	Gas to None
GR7	431.5	0.40	35	IV	None
GR8	431.2	0.74	115	III-IV	Gas to None
GR10	430.8	3.57	154	III	Gas
GR12	430.3	2.66	120	III	Gas
GR14	429.8	1.00	72	III	Gas
GR16	429.4	0.82	54	III-IV	Gas to None
GR18	428.8	1.17	84	III	Gas
GR20	428.4	1.01	72	III	Gas
GR22	427.6	1.27	69	III	Gas
GR24	427.1	0.87	51	III-IV	Gas to None
GR26	426.7	0.81	41	IV	None
GR X	424.0	0.52	35	IV	None
ME 001	441.3	0.08	28	IV	None
ME 003	450.9	0.39	67	III-IV	Gas to None
STB1	434.9	5.31	62	III-II/III	Gas to mixed oil -gas
STB3	436.4	4.51	181	III	Gas
STB5	437.4	0.41	31	IV	None
STB8	439.3	0.11	16	IV	None
SBG 2-33	407.0	0.75	37	IV	None
SBG 2-35	409.0	1.30	52	III	Gas
SBG 2-37	411.0	0.62	38	IV	None
SBG 2-39	413.0	0.61	35	IV	None
SBG 2-41	415.0	0.46	40	IV	None
SBG 2-42	417.0	0.38	36	IV	None
SBG 2-44	419.0	1.54	46	III-IV	Gas to None

Sample GR8 is type II/III kerogen with possible influence from altered organic matter and mineral matrix. ME003 displays a character such as GR8, but is also part of type III which is gas prone. GR1, STB3, GR10, GR12, STB1, GR22, GR18, GR14 and GR2 samples are type III kerogen which is gas prone. Samples that have lower HI than 50 mg HC/g TOC typified as inertinites. So, samples GR5, SBG2-44, SBG2-35, GR24 and GR16 are in an intermediate condition between type III and type IV kerogen. The rest of the samples are type IV which mean that are inertinites.

Finally, samples GR1 and STB1, with HI values lower than 300 mg HC/g TOC and S2/S3 ratio values higher than 5, display a type II/III character, which is an overestimation of the liquid hydrocarbon generative potential and the samples normally are type III. In addition, mineral matrix and alteration of organic matter are the possible effects for the misleading in the samples GR8 and ME003. GR8 is probably type III rather than type II/III and ME003 is type IV. The best samples in terms of kerogen **type are GR1, GR2, GR10, GR12, GR14, GR18, GR20, GR22, STB1, STB3, and SBG2-35 which show kerogen type III.** Noticeable influence of opaque phytoclasts (charcoals) are indicators of oxidation or high transportation and for that reason palynofacies must be taken into consideration in order to describe the kerogen type.

4.4.2 Quantity of organic matter

It is observed from Table 4.3, that three samples represent excellent to good petroleum potential source rocks: GR1, STB1 and STB3. They show high TOC and high S2, whereas S1 is very low and coincides with the poor category. TOC cannot be a good indicator for petroleum potential if it is consider alone, because the organic matter can be inert that is not generate petroleum (Peters and Cassa, 1994).

The diagram shows (Fig.4.15) that excellent petroleum potential have the samples GR1, STB1 and STB3, while samples GR2 and GR6 indicate very good character of petroleum potential. GR2, GR12 show good petroleum potential, too. Samples GR18, GR20, GR22, STB5 and GR7 have quiet high TOC but the S2 is very low. GR8, GR14, GR16, GR24, GRX, STB8 and the samples from SBG 2 section show fair TOC content but very low S2. ME001 and ME003 display poor petroleum potential character.

The samples GR1, STB1, STB3 show very good to excellent genetic potential with S2 values 10 mg HC/g rock. However, the rest samples are nonsource units as they lack of any significant hydrocarbon generative potential. The PP is below 2 mg HC/g rock.

It is conclude that the most prolific samples in terms of quantity- petroleum potential are **GR1, STB1** and **STB3** followed by samples **GR2**, **GR6, GR10** and **GR12**.

Table 4.3: The description of Petroleum Potential of the samples in terms of organic matter parameters (TOC, S2 from Rock-Eval pyrolysis), Bitumen and Hydrocarbons.

Sample	Depth(m)	TOC(%)	S2(mg HC/g rock)	PP=S1+S2	Petroleum Potential
GR1	432.9	5.35	10.73	10.86	Excellent and Very Good
GR2	432.2	2.25	1.58	1.65	Very Good and Poor
GR6	431.7	4.89	2.32	2.38	Excellent and Poor
GR7	431.5	1.26	0.44	0.47	Good and Poor
GR8	431.2	0.66	0.76	0.80	Fair and Poor
GR10	430.8	1.25	1.93	1.97	Good and Poor
GR12	430.3	1.24	1.49	1.53	Good and Poor
GR14	429.8	0.92	0.66	0.71	Fair and Poor
GR16	429.4	0.67	0.36	0.40	Fair and Poor
GR18	428.8	1.14	0.96	0.99	Good and Poor
GR20	428.4	1.33	0.96	1.04	Good and Poor
GR22	427.6	1.10	0.76	0.78	Good and Poor
GR24	427.1	0.93	0.47	0.50	Fair and Poor
GR26	426.7	1.02	0.42	0.45	Good and Poor
GR X	424.0	0.98	0.34	0.36	Fair and Poor
ME 001	441.3	0.22	0.06	0.08	Poor
ME 003	450.9	0.45	0.30	0.36	Poor
STB1	434.9	15.13	9.40	9.63	Excellent and Good
STB3	436.4	9.89	17.87	18.21	Excellent and Very Good
STB5	437.4	1.90	0.59	0.65	Good and Poor
STB8	439.3	0.61	0.10	0.13	Fair and Poor
SBG 2-33	407.0	0.81	0.30	0.33	Fair and Poor
SBG 2-35	409.0	0.93	0.48	0.53	Fair and Poor
SBG 2-37	411.0	0.81	0.31	0.32	Fair and Poor
SBG 2-39	413.0	0.71	0.25	0.28	Fair and Poor
SBG 2-41	415.0	0.89	0.35	0.39	Fair and Poor
SBG 2-42	417.0	0.79	0.28	0.29	Fair and Poor
SBG 2-44	419.0	0.81	0.37	0.40	Fair and Poor

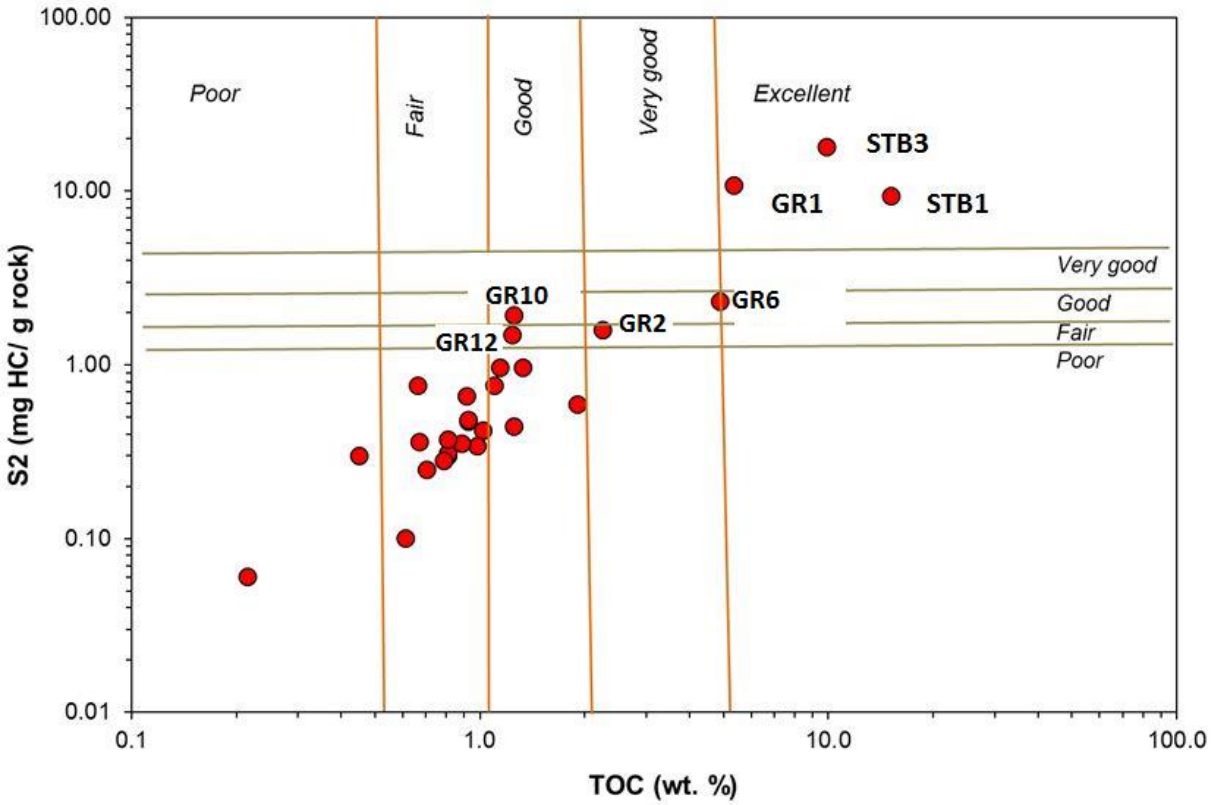

Fig. 4.15: The diagram shows the petroleum potential of the Carnian shales that were collected from Lunz am See, Austria.

4.4.3 Thermal maturity of organic matter

According to Peters and Cassa (1994), the interpretation of the maturity indices of the samples show that the organic material is mainly immature with respect to hydrocarbon generation (Table 4.4). These are the samples which are highlighted with yellow colour. Furthermore, the samples which are highlighted with green colour display immature to early mature- early/peak mature character, while only ME 001 (pink colour) shows an immature to peak mature character.

The diagram HI versus T_{max} shows most of the samples having equivalent vitrinite reflectance values approximately to 0.5% (Fig. 4.16). The samples correspond mostly to an immature character or/and an early mature.

Table 4.4: The samples are defined for their Thermal Maturation.

Sample	Depth(m)	Tmax(°C)	PI [S1/(S1+S2)]	Stages of Thermal Maturity for Oil
GR1	432.9	427	0.01	Immature
GR2	432.2	436	0.04	Early Mature to Immature
GR6	431.7	429	0.03	Immature
GR7	431.5	439	0.07	Early Mature to Immature
GR8	431.2	426	0.05	Immature
GR10	430.8	432	0.02	Immature
GR12	430.3	431	0.02	Immature
GR14	429.8	427	0.07	Immature
GR16	429.4	430	0.10	Immature to Early Mature
GR18	428.8	428	0.03	Immature
GR20	428.4	429	0.08	Immature
GR22	427.6	428	0.02	Immature
GR24	427.1	429	0.06	Immature
GR26	426.7	430	0.06	Immature
GR X	424.0	429	0.07	Immature
ME 001	441.3	427	0.27	Immature to Peak Mature
ME 003	450.9	434	0.16	Immature to Early Mature
STB1	434.9	427	0.02	Immature
STB3	436.4	430	0.02	Immature
STB5	437.4	426	0.09	Immature
STB8	439.3	262	0.23	Immature to Early/Peak Mature
SBG 2-33	407.0	434	0.08	Immature
SBG 2-35	409.0	436	0.09	Early Mature to Immature
SBG 2-37	411.0	434	0.03	Immature
SBG 2-39	413.0	432	0.12	Immature to Early Mature
SBG 2-41	415.0	433	0.10	Immature to Early Mature
SBG 2-42	417.0	436	0.05	Early Mature to Immature
SBG 2-44	419.0	434	0.08	Immature

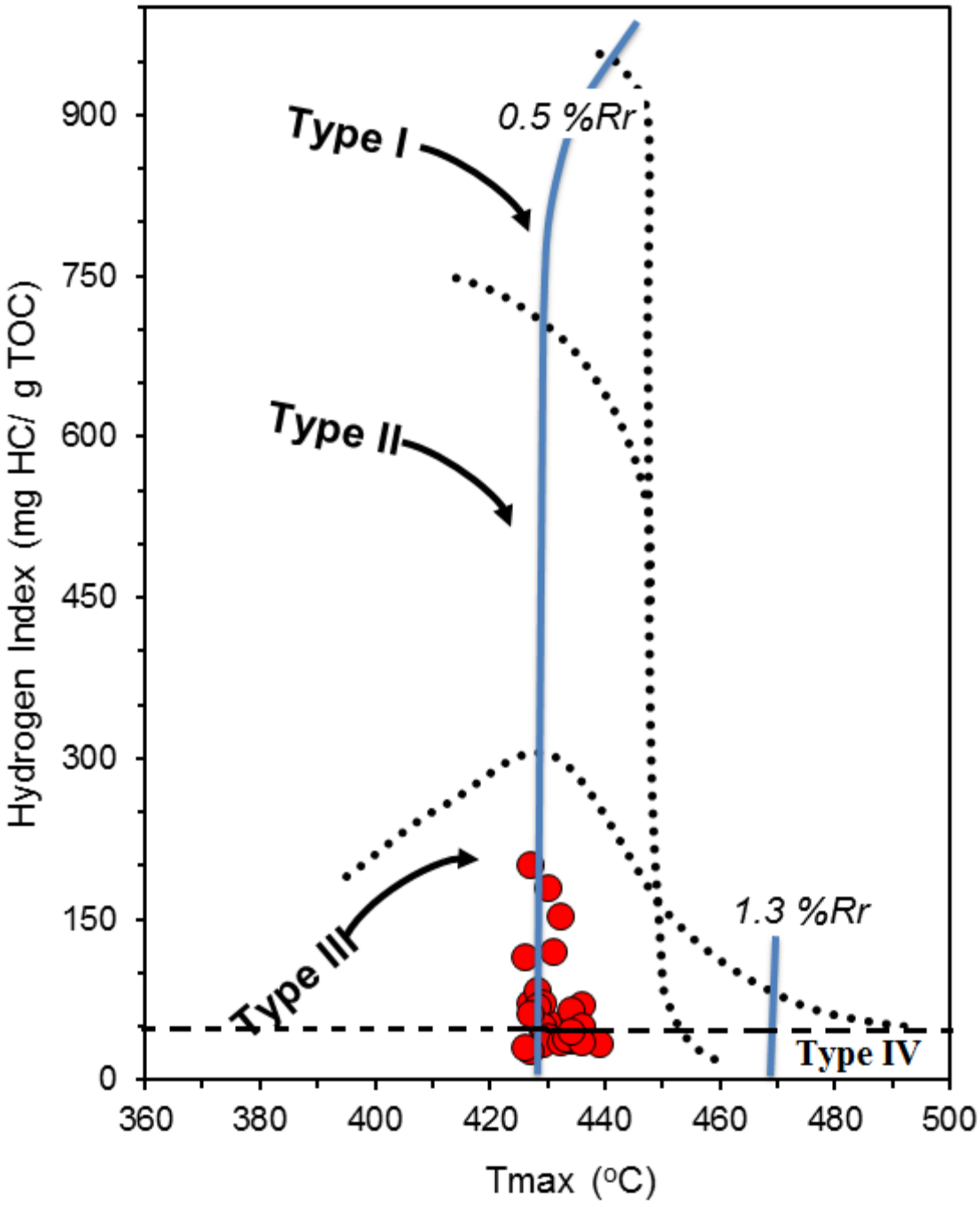

Fig. 4.16: The diagram HI versus Tmax. It is shown the type of kerogen and the thermal maturity of the samples.

5. Discussion

5.1 Palaeoenvironmental interpretation

The Steinbach , Grossreifling and Sulzbachgraben sections were deposited in a proximal neritic deep shelf area. A ternary diagram of AOM-Palynomorphs-Phytoclasts plot has been used to interpret the depositional environment. The samples plot in fields and the results are shown in Table 4.1.

The sediments of Reifling Formation are deposited within a proximal, deeper, low-energy marine basin setting in the NW Tethys margin (Hornung and Brandner, 2005). This study confirms this interpretation by the presence of *Tasmanites* sp., which is typical for a restricted marine depositional environments as well as reduced salinity waters and cooler waters (Prauss et al., 1991) together with the presence of marine acritarchs such as *Micrhystridium* spp.. However, the abundance of wood and the high equidimensional: lath-shaped opaque ratio indicates proximity to the fluvio-deltaic source (Tyson, 1993, Tyson, 1995).

The Göstling Member is characterized by calciturbidites (Hornung et al., 2007b)and is interpreted as being deposited in a distal dysoxic- anoxic setting of a basin in the shallow marine shelf at the northwestern rim of the Tethys. This has been verified by this study through dominant AOM with a minor increase in marine palynomorphs of acritarchs (*Micrhystridium* spp.), low salinity water prasinophytes, *Tasmanites* spp. and the first occurrence of *Cymatiosphaera* spp. The palynofacies analysis of lower Göstling Member shows that is strongly fluorescent, with algal inclusions of acritarchs. Therefore, the origin of the AOM is considered as algal or/and bacterial that indicates a low energy, stagnant and oxygen-depleted palaeoenvironment (Pacton et al., 2011). Mueller et al. (2015)conducted a micropalaeontological study of the Göstling Mb at Lunz am See and described an increase in marine palynomorphs. The negative excursion of $\delta^{13}C_{org}$ at the Julian 1-2 boundary, already reported by Dal Corso et al. (2012), (Dal Corso et al., 2015) may be related to changes in the biological source of the organic matter deposited into the basins (Kuerschner et al., 2007,

Smith et al., 2007, Van de Schootbrugge et al., 2008, French et al., 2014). Such a negative excursion has also been reported from Hungary (Baltonfüred) and the Southern Alps (Dolomites, Milieres section) (Dal Corso et al., 2015). Bonis et al. (2009) suggested that a negative $\delta^{13}C_{org}$ shift in the end-Triassic mass extinction displayed different phases in different depositional settings. A similar interpretation could be applied for the Carnian negative-carbon isotope excursion. The terrestrial and marine organic matter has different $\delta^{13}C_{org}$ signatures that result from their source of the organic carbon. There is an increase in terrigenous sediments at the onset of CPE. That might be connected to the changes in relative abundances of either marine or terrestrial organic matter in different basins, depending on the catchment area and the proximity of the section to the paleo-shoreline (Dal Corso et al., 2015). Dal Corso et al. (2012) suggest that the negative excursion of $\delta^{13}C_{org}$ could have been triggered by the volcanic activity of the Wragellia oceanic plateau in the America, yet the volcanic products could be overestimated and have been subducted in the Late Jurassic-Early Cretaceous (Lassiter et al., 1995, Greene et al., 2010). Their onset also appears to be earlier in the Ladinian (Xu et al., 2014). In the claystone interbeds of the Göstling Member, the TOC values are high and reach up 15% in the middle part of the member. This indicates oxygen-depletion that may have been caused by nutrient rich input into the basin as a result from enhanced continental weathering (Hornung et al., 2007a). The oxygen-depletion has been recorded in other basin across the Tethys such as in the Dolomites (Southern Italy) (Keim et al., 2006), in Tunisia(Soua, 2014), in the lower Rama Formation, in the Spiti Basin (India) (Hornung et al., 2007b), in the Hallstatt facies belt (Hornung and Brandner, 2005, Hornung et al., 2007c), and in the South China Block (Great Bank of Guizhou)(Xiaofeng et al., 2008).

The increase of rainfall resulted in an increase in fluvial delivered siliciclastics and allochthonous organic matter into the basin. The periodical increase in runoff from the continent caused a water stratification of the basin. This then led to the bottom waters to become anoxic and increased preservation of sedimentary organic matter. The high amount of AOM could be related to the high productivity of algae in the photic zone. When the algae die, bacteria- decomposers increase their activity and a further oxygen-depletion result at the basin floor bottoms (Fig. 5.1B). Oxygen-deficient conditions can be also caused by high

supply of land-plant derived organic matter (Fig. 5.1A). This enhances more the dysoxic conditions at the bottom waters during the formation of black shales.

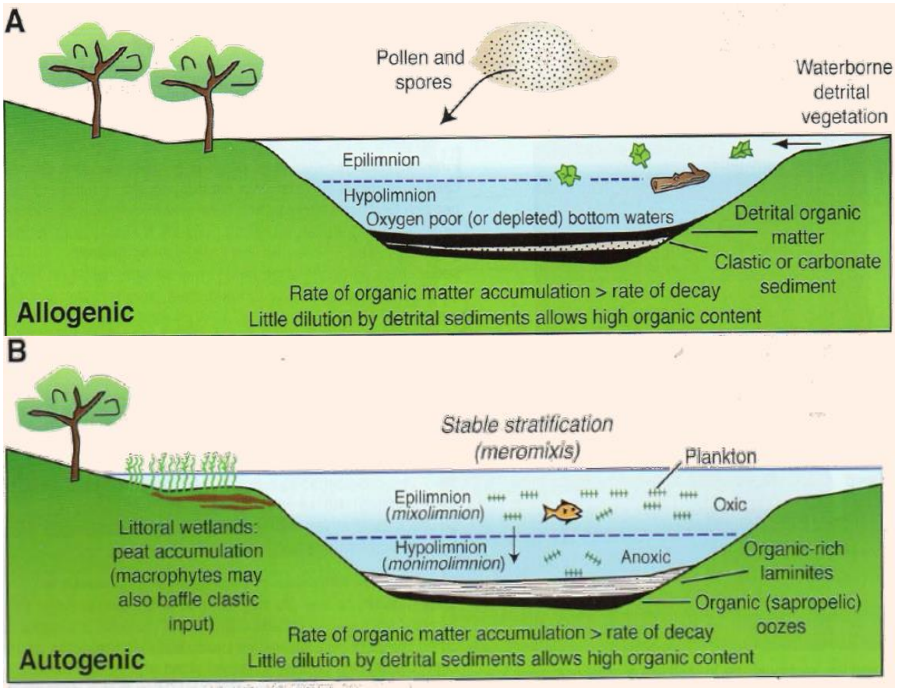

Fig. 5.1: Autogenic and allogenic supply of nutrients (Renaut and Gielowski-Kordesch, 2010).

The overlying Reingraben Formation was deposited in a proximal deep shelf setting with fluctuations in water depths due to variations in sedimentation rate and basin subsidence. This is indicated by the more oxic conditions in palynofacies 3, 5 and 7. There, phytoclasts and terrestrial palynomorphs are abundant compared to the small amount of AOM and marine palynomorphs. The existence of acritarchs such as *Micrhystridium* spp, and low salinity water prasinophytes (Prauss et al., 1991)(e.g. *Cymatiosphaera* spp. and *Tasmanites* spp.), foraminiferal test linings and scolecodonts indicate a marine influence throughout the lower part of the Reingraben Formation. However, the formation upwards is fresh water and terrestrially-dominated verified by the high relative abundance of degraded plant cuticles. The occasionally occurrence of the fresh water algae *Botryococcus* spp suggests low saline conditions.

The siliciclastic input accompanied with oxygen depletion decreases the carbonate production in basins in Austria and Hungary during the Carnian (Schlager and Schöllnberger, 1974, Simms and Ruffell, 1989, Hornung et al., 2007b). The carbonate system of Tethys experienced a crisis of carbonate production. As a consequence, the Carbonate Compensation Depth (CCD) rose as described in the Lagonegro Basin in the Southern Alps (Rigo et al., 2007). The high-relief carbonates platforms disappeared during the CPE (Preto and Hinnov, 2003, Keim et al., 2006, Stefani et al., 2010).The Göstling Member provides evidence for the demise of this microbial carbonate factory (Hornung et al., 2007a, Hornung et al., 2007c). The combination of a decrease in seawater saturation state relative to carbonate, the demise of microbial carbonate platforms in the Carnian and the corresponding negative carbon isotope excursion implies humid climate and fresh water input in the shelf.

5.1.1 Redox conditions

The ternary diagram of Tyson (1993) indicates the oxygen-depletion of the water column. The Reifling Formation is characterized by dysoxic to anoxic conditions. The formation consists of moderate amount of AOM but with an upwards increasing trend (Fig. 5.2). A similar trend has been observed in the TOC values. The Göstling Member is also characterized by a dysoxic to anoxic trend in redox conditions and is in agreement with the presence of high amount of AOM and the extremely high TOC (Fig. 5.2). The Reingraben Formation is described to be dysoxic to anoxic with two short periods of oxic to suboxic conditions due to temporary climatic variations (Bonis et al., 2010) controlling the fresh water influx into the saline basin . Higher up in the section is denoted by oxic conditions verifying from the very low AOM and TOC values (Fig. 5.2).

The presence of AOM content is owing to the better preservation in reducing environments (Ercegovac and Kostić, 2006, Pacton et al., 2011). Additionally, the granular type of AOM indicates anoxia showing that most of the degraded process is controlled by microbial activity under reducing conditions (Pacton et al., 2011).

The succession is rich in pyrite content and observed in forms of inclusions in AOM or individually (framboid pyrite) indicating oxygen-depleted environments (Tyson, 1995, Batten, 1996, Soua, 2014). The presence of foraminifera in the dysoxic-anoxic part of the

Reingraben Formation contradicts with the assumption that foraminifera prefer to flourish in oxic conditions (Tyson, 1995, Batten, 1996). However, some foraminifera could be allochthonous and were transported from the hinterland within a deltaic setting into anoxic environment, while in dysoxic condition environments might be characterized by autochthonous forms (Armstrong and Brasier, 2005).

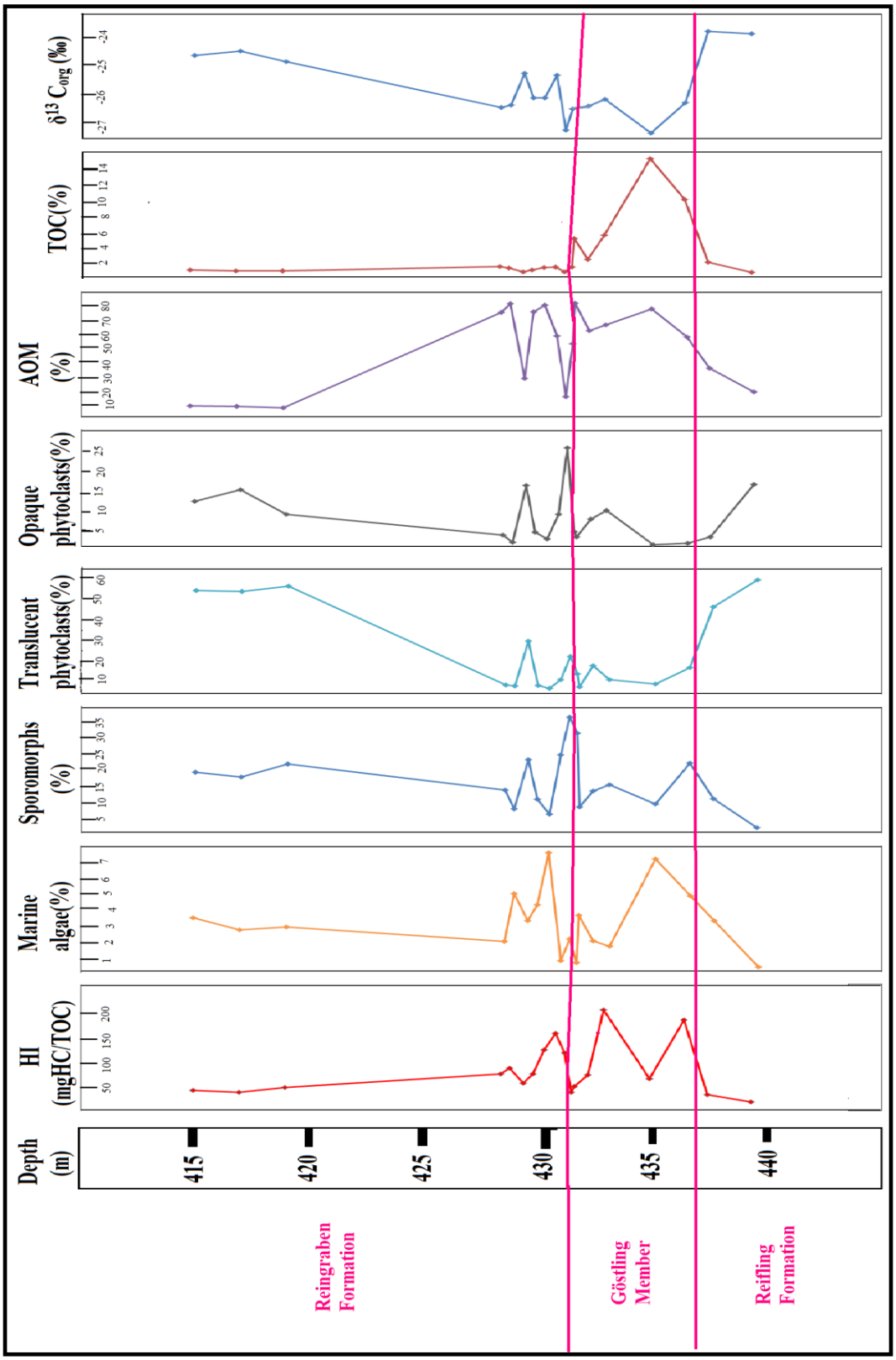

Fig. 5.2: The main palynofacies categories compared to HI, TOC and δ13Corg.

5.2 Source rock potential

Geochemical data combined with palynofacies analysis can indicate accurately the petroleum potential of sedimentary rocks (Batten, 1996). In particular, the correlation of palynofacies data along with TOC and HI can be used to evaluate the processes that are responsible for the hydrocarbon accumulation in sediments (Fig. 5.2) (Batten, 1996). Generally, the majority of studied source rocks have TOC values of less than 2% and are interpreted to be barren or contain only gas prone hydrocarbons (Traverse, 2007). Only few source rocks are economically important and have TOC values of more than 2% and are mainly gas prone. In addition, the source rocks are immature with Tmax values lower that 435°C and production index values lower than 0.1. Exceptionally few source rocks have early/peak mature character.

In the Reifling Formation, the clay intercalations are characterized by kerogen type IV which is considered as barren. However, palynofacies classification after Tyson (1993) indicates kerogen type III. The relative abundance of woods is high and show weak fluorescence indicating oxidized particles (Tyson, 1995). This type of oxidized woods are assumed the pre-form of opaque phytoclasts indicating inertinite.

The Göstling Member contains mudstone intervals that are characterized by kerogen III (gas prone). The Tyson (1993) palynofacies ternary diagram indicates mainly kerogen type II due to high concentrations of AOM and more marine algae than the other formations (Tasmanites, acritarchs). Rocks in the Göstling Member show excellent to good hydrocarbon potential. The TOC values reach up to15% in the lower part of the Member. Batten (1996) assumes that it is a rare phenomenon that sequences contain more than 10% TOC. Hetényi et al. (2004) suggest that high TOC is caused by high productivity, when the climate-induced weathering influx increased. The HI is very low. This misleading is explained by the high weathering outcrops where the samples were taken. However, the TOC content alone is not the only indicator for determining the petroleum potential (Karakitsios and Rigakis, 2007). Important role plays the thickness of the source rock unit assuming that thin Oceanic Anoxic Event (OAE) intervals, even very rich in organic matter, cannot be considered as source rocks (Karakitsios and Rigakis, 2007). Consequently, the source rock intervals at the lower

Göstling Mb with extremely high TOC are prevented from generating volumes of hydrocarbons substantially due to the limited thicknesses.

The organic rich shales of the Reingraben Formation contain two intervals with high AOM accompanied by relative high amounts of aquatic algae that corresponded to P4 and P6 (Fig. 5.2). Both assemblages have high HI and the geochemical interpretation indicates a type III kerogen. Palynofacies show kerogen type II. This discrepancy may have been caused by the preservation state of the samples. Outcrop samples usually have depleted S2 and S1 and high S3 due to weathering (Peters, 1986), thus influence the HI indicating low values. Nevertheless, the TOC is lower than 2% verifying that these shale intervals could potentially generate only small gaseous amounts of hydrocarbons. The remainder of the shales of the Reingraben Formation is characterized by poor source rock quality and is a type IV kerogen. These samples contain mainly translucent phytoclasts which are weakly fluorescent and indicate that they are oxidized particles.

The Carnian shales in Tunisia are assumed good source rocks of kerogen type II and III (Soua, 2014)showing similarities to Carnian successions from Germanic, southern Alps (Katz et al., 2000, Cirilli et al., 2015), southern Apennines and Po basins.

5.3 Comparison of the carbon isotope excursion (CIE) with another site.

The CIE in the bulk organic matter at Lunz am See and Kuhjoch, in Austria, established at the Julian1-2 and Triassic-Jurassic boundaries, respectively. The comparison of the curves of $\delta^{13}C_{org}$ can be done in combination with the organic matter. The two CIE have different orders of magnitudes (Fig. 5.3). At Lunz the negative excursion is about 3-4%, while at Kuhjoch it is 2%-7% (Ruhl et al., 2010). Figure 5.2 shows that the observed CIE shifts to more negative values when the organic matter contains high AOM and aquatic algae, while phytoclasts and sporomorphs are low. The differences from positive to negative CIE could be related to a change in the biological source of the organic matter in the basin (Kuerschner et al., 2007, French et al., 2014). According to Ruhl et al. (2010), the different magnitudes indicate different depositional environments. It can be used as distal-proximal indicator.

The initiation of the negative CIE at Lunz am See corresponds to the onset of the CPE, whereas the initiation of negative CIE related to the starting period of the end-Triassic mass extinction. Both successions are related to black shale deposition and the demise of carbonate sedimentation. The occurrence of prasinophytes in the black shales is usual (Bonis et al., 2010). They indicate the influence of fresh water in a marine setting in the stagnant marine basins of the Eiberg Basin (Bonis et al., 2010) as well as in the Reifling basin. The occurrence of prasinophytes show high relative abundances together with acritarchs during the CPE, while the $\delta^{13}C_{org}$ has a negative excursion (Fig. 5.2). This indicates that these aquatic algae are good climatological and/or oceanographic control (Prauss and Riegel, 1989, Bonis et al., 2010). The similar negative CIE of the black shales in the Kuhjoch area coincides with the occurrence of prasinophytes (Ruhl et al., 2010). The two negative CIE seems to be connected showing similar environmental conditions.

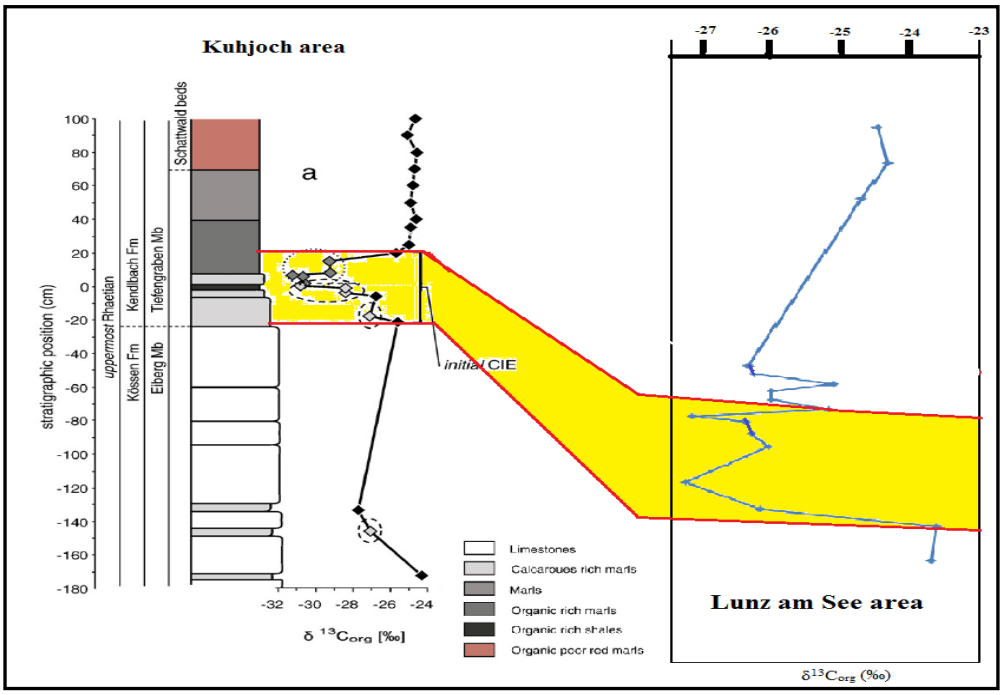

Fig. 5.3: Comparison of the negative CIE between Kuhjoch and Lunz am See area (modified after Ruhl et al., 2010).

6. Conclusions

This study was conducted with the purpose to understand the environmental conditions and the controlling factors of the deposition of black shales during the Carnian Pluvial Event (CPE). The palynofacies and geochemical data analysis of the retrieved samples from the Lower Carnian shale interval yielded the following conclusions:

1. The composition of particulate organic matter in Reifling Formation, Göstling Member and Reingraben Formation suggests that the sediments were deposited in a neritic shelf close to the shoreline.

2. The redox conditions are indicated mainly as dysoxic-anoxic with some changes to more suboxic-oxic conditions. However, the succession turns to oxic conditions upwards.

3. High algal productivity was due to influx of nutrients into the basin caused by the eutrophication phenomenon and consequent high bacterial decomposers. This explains the high values of TOC in the Göstling Member.

4. From the scope of source rocks, they are kerogen type III and kerogen type IV, and are further limit by their extreme weathering. The mineral matrix influence leads to misinterpretations. Palynofacies deviates from geochemical data indicating more prolific source rocks.

5. The high TOC values of the Göstling Member and the Reingraben Formation show good to excellent petroleum potential. However, the Göstling Member is prevented from being an economic source rocks by its limited thickness.

6. The source rocks display immature character with a minority having early mature to peak mature character.

7. The onset of the negative carbon isotope excursion coincides with the onset of a humid period, the Carnian Pluvial Event. The change from positive to negative indicates correspondence to changes in organic matter in the shales.

8. The occurrence of prasinophytes coincides with the deposition of black shales in the Carnian as well as in the Triassic-Jurassic boundary indicating climatological shifts.

7. Acknowledgements

I would like to thank my supervisor Wolfram M. Kürschner for his guidance and his valuable advices through palynology and upon the use of fluorescent and transmitted light microscope. I also would like to thank Steven Mueller who supplies me with the palynological slides and the $\delta^{13}C_{org}$ data, which are part of his PhD project and his support in making the graphs in Tilia and generally his advices for the present report. Thanks also go to my friends who support me in the difficulties I faced throughout the whole academic year and for always believing in me and giving me courage to continue. Finally, I would like to thank my family for their support throughout my studies.

8. References

ARCHE, A. & LÓPEZ-GÓMEZ, J. 2014. The Carnian Pluvial Event in Western Europe: new data from Iberia and correlation with the Western Neotethys and Eastern North America–NW Africa regions. *Earth-Science Reviews,* 128**,** 196-231.

ARMSTRONG, H. A. & BRASIER, M. D. 2005. Microfossils, Stable Isotopes and Ocean-Atmosphere History. *Microfossils, Second Edition***,** 25-34.

BATTEN, D. 1996. Palynofacies and palaeoenvironmental interpretation. *Palynology: principles and applications,* 3**,** 1011-1064.

BIALIK, O. M., KORNGREEN, D. & BENJAMINI, C. 2013. Carnian (Triassic) aridization on the Levant margin: evidence from the M1 member, Mohilla Formation, Makhtesh Ramon, south Israel. *Facies,* 59**,** 559-581.

BLAKEY, R. 2011. Global paleogeography. NAU Geology.

BONIS, N., KÜRSCHNER, W. & KRYSTYN, L. 2009. A detailed palynological study of the Triassic–Jurassic transition in key sections of the Eiberg Basin (Northern Calcareous Alps, Austria). *Review of Palaeobotany and Palynology,* 156**,** 376-400.

BONIS, N., RUHL, M. & KÜRSCHNER, W. 2010. Climate change driven black shale deposition during the end-Triassic in the western Tethys. *Palaeogeography, Palaeoclimatology, Palaeoecology,* 290**,** 151-159.

BREDA, A., PRETO, N., ROGHI, G., FURIN, S., MENEGUOLO, R., RAGAZZI, E., FEDELE, P. & GIANOLLA, P. 2009. The Carnian Pluvial Event in the Tofane area (Cortina d'Ampezzo, Dolomites, Italy). *Geo Alp,* 6**,** 80-115.

BUDUROV, K. & STEFANOV, S. 1965. Gattung Gondolella aus der Trias Bulgariens. *Doklady Bolgarskoy Akademiya Nauk, Série Paléontologie,* 7**,** 115-127.

CIRILLI, S., BURATTI, N., GUGLIOTTI, L. & FRIXA, A. 2015. Palynostratigraphy and palynofacies of the Upper Triassic Streppenosa Formation (SE Sicily, Italy) and inference on the main controlling factors in the organic rich shale deposition. *Review of Palaeobotany and Palynology*.

COMBAZ, A. 1964. Les palynofacies. *Revue de Micropaléontologie,* 7**,** 205-218.

DAL CORSO, J., GIANOLLA, P., NEWTON, R. J., FRANCESCHI, M., ROGHI, G., CAGGIATI, M., RAUCSIK, B., BUDAI, T., HAAS, J. & PRETO, N. 2015. Carbon isotope records reveal synchronicity between carbon cycle perturbation and the "Carnian Pluvial Event" in the Tethys realm (Late Triassic). *Global and Planetary Change,* 127**,** 79-90.

DAL CORSO, J., MIETTO, P., NEWTON, R. J., PANCOST, R. D., PRETO, N., ROGHI, G. & WIGNALL, P. B. 2012. Discovery of a major negative δ13C spike in the Carnian (Late Triassic) linked to the eruption of Wrangellia flood basalts. *Geology,* 40**,** 79-82.

DUBIEL, R. F., PARRISH, J. T., PARRISH, J. M. & GOOD, S. C. 1991. The Pangaean megamonsoon: evidence from the Upper Triassic Chinle Formation, Colorado Plateau. *Palaios***,** 347-370.

ERCEGOVAC, M. & KOSTIĆ, A. 2006. Organic facies and palynofacies: nomenclature, classification and applicability for petroleum source rock evaluation. *International Journal of Coal Geology,* 68**,** 70-78.

ESPITALIÉ, J. 1986. Use of Tmax as a maturation index for different types of organic matter. Comparison with vitrinite reflectance. *Thermal modelling in sedimentary basins.* Editions Technip Paris.
ESPITALIE, J., DEROO, G. & MARQUIS, F. 1985. Rock-Eval pyrolysis and its applications. *Revue De L Institut Francais Du Petrole,* 40**,** 563-579.
ESPITALIE, J., MADEC, M., TISSOT, B., MENNIG, J. & LEPLAT, P. Source rock characterization method for petroleum exploration. Offshore Technology Conference, 1977. Offshore Technology Conference.
FRENCH, K. L., SEPULVEDA, J., TRABUCHO-ALEXANDRE, J., GRÖCKE, D. & SUMMONS, R. E. 2014. Organic geochemistry of the early Toarcian oceanic anoxic event in Hawsker Bottoms, Yorkshire, England. *Earth and Planetary Science Letters,* 390**,** 116-127.
GALLET, Y., BESSE, J., KRYSTYN, L., THÉVENIAUT, H. & MARCOUX, J. 1994. Magnetostratigraphy of the Mayerling section (Austria) and Erenkolu Mezarlik (Turkey) section: Improvement of the Carnian (late Triassic) magnetic polarity time scale. *Earth and planetary science letters,* 125**,** 173-191.
GOLONKA, J. 2002. Plate-tectonic maps of the Phanerozoic.
GOLONKA, J. 2004. Plate tectonic evolution of the southern margin of Eurasia in the Mesozoic and Cenozoic. *Tectonophysics,* 381**,** 235-273.
GOLONKA, J. 2007. Late Triassic and Early Jurassic palaeogeography of the world. *Palaeogeography, Palaeoclimatology, Palaeoecology,* 244**,** 297-307.
GOLONKA, J. & FORD, D. 2000. Pangean (late Carboniferous–Middle Jurassic) paleoenvironment and lithofacies. *Palaeogeography, Palaeoclimatology, Palaeoecology,* 161**,** 1-34.
GREENE, A. R., SCOATES, J. S., WEIS, D., KATVALA, E. C., ISRAEL, S. & NIXON, G. T. 2010. The architecture of oceanic plateaus revealed by the volcanic stratigraphy of the accreted Wrangellia oceanic plateau. *Geosphere,* 6**,** 47-73.
HAAS, J., BUDAI, T. & RAUCSIK, B. 2012. Climatic controls on sedimentary environments in the Triassic of the Transdanubian Range (Western Hungary). *Palaeogeography, Palaeoclimatology, Palaeoecology,* 353**,** 31-44.
HAAS, J. & DEMÉNY, A. 2002. Early dolomitisation of Late Triassic platform carbonates in the Transdanubian Range (Hungary). *sedimentary Geology,* 151**,** 225-242.
HALLAM, A. 1985. A review of Mesozoic climates. *Journal of the Geological Society,* 142**,** 433-445.
HALLAM, A. & WIGNALL, P. 1999. Mass extinctions and sea-level changes. *Earth-Science Reviews,* 48**,** 217-250.
HESSELBO, S. P., ROBINSON, S. A., SURLYK, F. & PIASECKI, S. 2002. Terrestrial and marine extinction at the Triassic-Jurassic boundary synchronized with major carbon-cycle perturbation: A link to initiation of massive volcanism? *Geology,* 30**,** 251-254.
HORNUNG, T. & BRANDNER, R. 2005. Biochronostratigraphy of the Reingraben Turnover (Hallstatt Facies Belt): Local black shale events controlled by regional tectonics, climatic change and plate tectonics. *Facies,* 51**,** 460-479.
HORNUNG, T., BRANDNER, R. & KRYSTYN, L. Carnian black shale events triggered by Cimmerian-Eurasian collision? Geophysical Research Abstracts, 2005. 04057.
HORNUNG, T., BRANDNER, R., KRYSTYN, L., JOACHIMSKI, M. M. & KEIM, L. 2007a. Multistratigraphic constraints on the NW Tethyan "Carnian crisis". *The Global Triassic,* 41**,** 59-67.

HORNUNG, T., KRYSTYN, L. & BRANDNER, R. 2007b. A Tethys-wide mid-Carnian (Upper Triassic) carbonate productivity crisis: Evidence for the Alpine Reingraben Event from Spiti (Indian Himalaya)? *Journal of Asian Earth Sciences,* 30**,** 285-302.
HORNUNG, T., SPATZENEGGER, A. & JOACHIMSKI, M. M. 2007c. Multistratigraphy of condensed ammonoid beds of the Rappoltstein (Berchtesgaden, southern Germany): unravelling palaeoenvironmental conditions on 'Hallstatt deep swells' during the Reingraben Event (Late Lower Carnian). *Facies,* 53**,** 267-292.
JACQUIN, T. 1998. Major transgressive/regressive cycles: the stratigraphic signature of European basin development.
KARAKITSIOS, V. & RIGAKIS, N. 2007. Evolution and petroleum potential of Western Greece. *Journal of Petroleum Geology,* 30**,** 197-218.
KATZ, B., DITTMAR, E. & EHRET, G. 2000. A geochemical review of carbonate source rocks in Italy. *Journal of Petroleum Geology,* 23**,** 399-424.
KEIM, L., BRANDNER, R., KRYSTYN, L. & METTE, W. 2001. Termination of carbonate slope progradation: an example from the Carnian of the Dolomites, Northern Italy. *Sedimentary Geology,* 143**,** 303-323.
KEIM, L., SPÖTL, C. & BRANDNER, R. 2006. The aftermath of the Carnian carbonate platform demise: a basinal perspective (Dolomites, Southern Alps). *Sedimentology,* 53**,** 361-386.
KIDDER, D. L. & WORSLEY, T. R. 2004. Causes and consequences of extreme Permo-Triassic warming to globally equable climate and relation to the Permo-Triassic extinction and recovery. *Palaeogeography, Palaeoclimatology, Palaeoecology,* 203**,** 207-237.
KORTE, C., HESSELBO, S. P., JENKYNS, H. C., RICKABY, R. E. & SPÖTL, C. 2009. Palaeoenvironmental significance of carbon-and oxygen-isotope stratigraphy of marine Triassic–Jurassic boundary sections in SW Britain. *Journal of the Geological Society,* 166**,** 431-445.
KORTE, C., KOZUR, H. W. & VEIZER, J. 2005. δ 13 C and δ 18 O values of Triassic brachiopods and carbonate rocks as proxies for coeval seawater and palaeotemperature. *Palaeogeography, Palaeoclimatology, Palaeoecology,* 226**,** 287-306.
KOZUR, H. 2003. Integrated Permian ammonoid, conodont, fusulinid, marine ostracod and radiolarian biostratigraphy. *Permophiles,* 42**,** 24-33.
KRYSTYN, L. 1980. Triassic conodont localities of the Salzkammergut region. *Abh. Geol. B.-A,* 35**,** 61-98.
KRYSTYN, L. 1983. Das Epidaurus-Profil (Griechenland)—ein Beitrag zur Conodonten-Standardzonierung des tethyalen Ladin und Unterkarn. *Neue Beiträge zur Biostratigraphie der Tethys-Trias. Schriftenr. erdwiss. Komm. österr. Akad. Wiss,* 5**,** 231-258.
KRYSTYN, L., GALLET, Y., BESSE, J. & MARCOUX, J. 2002. Integrated Upper Carnian to Lower Norian biochronology and implications for the Upper Triassic magnetic polarity time scale. *Earth and Planetary Science Letters,* 203**,** 343-351.
KUERSCHNER, W. M., BONIS, N. R. & KRYSTYN, L. 2007. Carbon-isotope stratigraphy and palynostratigraphy of the Triassic–Jurassic transition in the Tiefengraben section—Northern Calcareous Alps (Austria). *Palaeogeography, Palaeoclimatology, Palaeoecology,* 244**,** 257-280.

KUTZBACH, J. & GALLIMORE, R. 1989. Pangaean climates: megamonsoons of the megacontinent. *Journal of Geophysical Research: Atmospheres (1984–2012),* 94**,** 3341-3357.

KÜRSCHNER, W. M. & HERNGREEN, G. W. 2010. Triassic palynology of central and northwestern Europe: a review of palynofloral diversity patterns and biostratigraphic subdivisions. *Geological Society, London, Special Publications,* 334**,** 263-283.

LASSITER, J., DEPAOLO, D. & MAHONEY, J. 1995. Geochemistry of the Wrangellia flood basalt province: Implications for the role of continental and oceanic lithosphere in flood basalt genesis. *Journal of Petrology,* 36**,** 983-1009.

LOOPE, D., EISENBERG, L. & WAISS, E. 2004. Navajo sand sea of near-equatorial Pangea: Tropical westerlies, slumps, and giant stromatolites. *Field Guides,* 5**,** 1-13.

LORENTE, M. 1990. TEXTURAL CHARACTERISTICS OF ORGANIC-MATTER IN SEVERAL SUBENVIRONMENTS OF THE ORINOCO UPPER DELTA. *Geologie en Mijnbouw,* 69**,** 263-278.

LUKENEDER, S., LUKENEDER, A., HARZHAUSER, M., İSLAMOĞLU, Y., KRYSTYN, L. & LEIN, R. 2012. A delayed carbonate factory breakdown during the Tethyan-wide Carnian Pluvial Episode along the Cimmerian terranes (Taurus, Turkey). *Facies,* 58**,** 279-296.

MANDL, G. W. 2000. The Alpine sector of the Tethyan shelf—examples of Triassic to Jurassic sedimentation and deformation from the Northern Calcareous Alps. *Mitteilungen der Österreichischen Geologischen Gesellschaft,* 92**,** 61-77.

MARZOLI, A., BERTRAND, H., KNIGHT, K. B., CIRILLI, S., BURATTI, N., VÉRATI, C., NOMADE, S., RENNE, P. R., YOUBI, N. & MARTINI, R. 2004. Synchrony of the Central Atlantic magmatic province and the Triassic-Jurassic boundary climatic and biotic crisis. *Geology,* 32**,** 973-976.

MCELWAIN, J., BEERLING, D. & WOODWARD, F. 1999. Fossil plants and global warming at the Triassic-Jurassic boundary. *Science,* 285**,** 1386-1390.

MCELWAIN, J. C. & PUNYASENA, S. W. 2007. Mass extinction events and the plant fossil record. *Trends in Ecology & Evolution,* 22**,** 548-557.

MUELLER, S., KRYSTYN, L. & KÜRSCHNER, W. M. 2015. Climate variability during the Carnian Pluvial Phase–a quantitative palynological study of the Carnian sedimentary succession at Lunz am See, Northern Calcareous Alps, Austria. *Palaeogeography, Palaeoclimatology, Palaeoecology*.

MUELLER, S., VELD, H., NAGY, J. & KÜRSCHNER, W. M. 2014. Depositional history of the Upper Triassic Kapp Toscana Group on Svalbard, Norway, inferred from palynofacies analysis and organic geochemistry. *Sedimentary Geology,* 310**,** 16-29.

MUTTI, M. & WEISSERT, H. 1995. Triassic monsoonal climate and its signature in Ladinian-Carnian carbonate platforms (Southern Alps, Italy). *Journal of Sedimentary Research,* 65.

NAKADA, R., OGAWA, K., SUZUKI, N., TAKAHASHI, S. & TAKAHASHI, Y. 2014. Late Triassic compositional changes of aeolian dusts in the pelagic Panthalassa: Response to the continental climatic change. *Palaeogeography, Palaeoclimatology, Palaeoecology,* 393**,** 61-75.

OLSEN, P. E. & KENT, D. V. High-resolution early Mesozoic Pangean climatic transect in lacustrine environments. Epicontinental Triassic: International Symposium Halle/Saale, September 21-23, 1998, vol. 3, 2000. E. Schweizerbart'sche Verlagsbuchhandlung, 1475-1495.

PACTON, M., GORIN, G. E. & VASCONCELOS, C. 2011. Amorphous organic matter—Experimental data on formation and the role of microbes. *Review of Palaeobotany and Palynology,* 166**,** 253-267.
PARRISH, J. T. 1993. Climate of the supercontinent Pangea. *The Journal of Geology***,** 215-233.
PARRISH, J. T. & PETERSON, F. 1988. Wind directions predicted from global circulation models and wind directions determined from eolian sandstones of the western United States—A comparison. *Sedimentary Geology,* 56**,** 261-282.
PETERS, K. 1986. Guidelines for evaluating petroleum source rock using programmed pyrolysis. *AAPG bulletin,* 70**,** 318-329.
PETERS, K. E. & CASSA, M. R. 1994. Applied source rock geochemistry. *Memoirs-American Association of Petroleum Geologists***,** 93-93.
PRAUSS, M., LIGOUIS, B. & LUTERBACHER, H. 1991. Organic matter and palynomorphs in the 'Posidonienschiefer'(Toarcian, Lower Jurassic) of southern Germany. *Geological Society, London, Special Publications,* 58**,** 335-351.
PRAUSS, M. & RIEGEL, W. 1989. Evidence from phytoplankton associations for causes of black shale formation in epicontinental seas. *Neues Jahrbuch für Geologie und Paläontologie, Monatshefte,* 11**,** 671-682.
PRETO, N. & HINNOV, L. A. 2003. Unraveling the origin of carbonate platform cyclothems in the Upper Triassic Durrenstein Formation (Dolomites, Italy). *Journal of Sedimentary Research,* 73**,** 774-789.
PRETO, N., KUSTATSCHER, E. & WIGNALL, P. B. 2010. Triassic climates—state of the art and perspectives. *Palaeogeography, Palaeoclimatology, Palaeoecology,* 290**,** 1-10.
RIGO, M., PRETO, N., ROGHI, G., TATEO, F. & MIETTO, P. 2007. A rise in the carbonate compensation depth of western Tethys in the Carnian (Late Triassic): deep-water evidence for the Carnian Pluvial Event. *Palaeogeography, Palaeoclimatology, Palaeoecology,* 246**,** 188-205.
ROBINSON, P. L. 1973. Palaeoclimatology and continental drift. *Implications of continental drift to the earth sciences,* 1**,** 451-476.
ROGHI, G., GIANOLLA, P., MINARELLI, L., PILATI, C. & PRETO, N. 2010. Palynological correlation of Carnian humid pulses throughout western Tethys. *Palaeogeography, Palaeoclimatology, Palaeoecology,* 290**,** 89-106.
ROSTÁSI, Á., RAUCSIK, B. & VARGA, A. 2011. Palaeoenvironmental controls on the clay mineralogy of Carnian sections from the Transdanubian Range (Hungary). *Palaeogeography, Palaeoclimatology, Palaeoecology,* 300**,** 101-112.
RUHL, M., VELD, H. & KÜRSCHNER, W. 2010. Sedimentary organic matter characterization of the Triassic–Jurassic boundary GSSP at Kuhjoch (Austria). *Earth and Planetary Science Letters,* 292**,** 17-26.
SCHLAGER, W. & SCHÖLLNBERGER, W. 1974. Das Prinzip stratigraphischer Wenden in der Schichtfolge der Nördlichen Kalkalpen. *Mitt. Geol. Ges. Wien,* 66**,** 165-193.
SELLWOOD, B. W. & VALDES, P. J. 2006. Mesozoic climates: General circulation models and the rock record. *Sedimentary geology,* 190**,** 269-287.
SENGOR, A. & NATALIN, B. 1996. Paleotectonics of Asia: fragments of a synthesis.
SENGÖR, A. & HSÜ, K. 1984. The Cimmerides of eastern Asia: history of the eastern end of Paleo-Tethys. *Mem. Soc. Geol. France,* 147**,** 139-167.

ŞENGÖR, A. C. 1984. The Cimmeride orogenic system and the tectonics of Eurasia. *Geological Society of America Special Papers,* 195**,** 1-74.
SIMMS, M. J., RUFFEL, A., JOHNSON, L., FRASER, N. & SUES, H. 1995. Biotic and climatic changes in the Carnian (Triassic) of Europe and adjacent areas. *In the Shadow of the Dinosaurs: Early Mesozoic Tetrapods.* Cambridge University Press Cambridge,, UK.
SIMMS, M. J. & RUFFELL, A. H. 1989. Synchroneity of climatic change and extinctions in the Late Triassic. *Geology,* 17**,** 265-268.
SIMMS, M. J. & RUFFELL, A. H. 1990. Climatic and biotic change in the Late Triassic. *Journal of the Geological Society,* 147**,** 321-327.
SMITH, F. A., WING, S. L. & FREEMAN, K. H. 2007. Magnitude of the carbon isotope excursion at the Paleocene–Eocene thermal maximum: The role of plant community change. *Earth and Planetary Science Letters,* 262**,** 50-65.
SOUA, M. 2014. Early Carnian anoxic event as recorded in the southern Tethyan margin, Tunisia: an overview. *International Geology Review,* 56**,** 1884-1905.
SPALLETTI, L., ARTABE, A. & MOREL, E. 2003. Geological factors and evolution of southwestern Gondwana Triassic plants. *Gondwana Research,* 6**,** 119-134.
STAPLIN, F. 1982. Determination of thermal alteration index from color of exinite (pollen, spores).
STEFANI, M., FURIN, S. & GIANOLLA, P. 2010. The changing climate framework and depositional dynamics of Triassic carbonate platforms from the Dolomites. *Palaeogeography, Palaeoclimatology, Palaeoecology,* 290**,** 43-57.
TISSOT, B., DURAND, B., ESPITALIE, J. & COMBAZ, A. 1974. Influence of nature and diagenesis of organic matter in formation of petroleum. *AAPG Bulletin,* 58**,** 499-506.
TISSOT, B. P. & WELTE, D. H. 1984. Petroleum formation and occurrence.
TRAVERSE, A. 2007. *Differential Sorting of Palynomorphs into Sediments: Palynofacies, Palynodebris, Discordant Palynomorphs,* Springer.
TYSON, R. 1989. Late Jurassic palynofacies trends, Piper and Kimmeridge Clay formations, UK onshore and northern North Sea. *Northwest European micropalaeontology and palynology***,** 135-72.
TYSON, R. 1995. Sedimentary organic matter: organic facies and palynofaciesChapman and Hall. *London, New York.*
TYSON, R. V. 1993. Palynofacies analysis. *Applied micropalaeontology.* Springer.
VAN DE SCHOOTBRUGGE, B., PAYNE, J., TOMASOVYCH, A., PROSS, J., FIEBIG, J., BENBRAHIM, M., FÖLLMI, K. B. & QUAN, T. 2008. Carbon cycle perturbation and stabilization in the wake of the Triassic-Jurassic boundary mass-extinction event. *Geochemistry, Geophysics, Geosystems,* 9.
VAN DE SCHOOTBRUGGE, B., QUAN, T., LINDSTRÖM, S., PÜTTMANN, W., HEUNISCH, C., PROSS, J., FIEBIG, J., PETSCHICK, R., RÖHLING, H.-G. & RICHOZ, S. 2009. Floral changes across the Triassic/Jurassic boundary linked to flood basalt volcanism. *Nature Geoscience,* 2**,** 589-594.
VAN DER ZWAN, C. 1990. Palynostratigraphy and palynofacies reconstruction of the Upper Jurassic to lowermost Cretaceous of the Draugen Field, offshore Mid Norway. *Review of palaeobotany and palynology,* 62**,** 157-186.
VEEVERS, J. 2004. Gondwanaland from 650–500 Ma assembly through 320 Ma merger in Pangea to 185–100 Ma breakup: supercontinental tectonics via stratigraphy and radiometric dating. *Earth-Science Reviews,* 68**,** 1-132.

WANG, P. 2009. Global monsoon in a geological perspective. *Chinese Science Bulletin,* 54**,** 1113-1136.

WINN, W. 1993. An account of how readers search for information in diagrams. *Contemporary Educational Psychology,* 18**,** 162-185.

WITHJACK, M. O., SCHLISCHE, R. W. & OLSEN, P. E. 1998. Diachronous rifting, drifting, and inversion on the passive margin of central eastern North America: an analog for other passive margins. *AAPG bulletin,* 82**,** 817-835.

XIAOFENG, W., BACHMANN, G. H., HAGDORN, H., SANDER, P., CUNY, G., XIAOHONG, C., CHUANSHANG, W., LIDE, C., LONG, C. & FANSONG, M. 2008. THE LATE TRIASSIC BLACK SHALES OF THE GUANLING AREA, GUIZHOU PROVINCE, SOUTH-WEST CHINA: A UNIQUE MARINE REPTILE AND PELAGIC CRINOID FOSSIL LAGERSTÄTTE. *Palaeontology,* 51**,** 27-61.

XU, G., HANNAH, J. L., STEIN, H. J., MØRK, A., VIGRAN, J. O., BINGEN, B., SCHUTT, D. L. & LUNDSCHIEN, B. A. 2014. Cause of Upper Triassic climate crisis revealed by Re–Os geochemistry of Boreal black shales. *Palaeogeography, Palaeoclimatology, Palaeoecology,* 395**,** 222-232.

ZIEGLER, P. A. 1988. EVOLUTION OF THE ARCTIC-NORTH ATLANTIC AND THE WESTERN TETHYS--A VISUAL PRESENTATION OF A SERIES OF PALEOGEOGRAPHIC-PALEOTECTONIC MAPS*. *AAPG memoir,* 43**,** 164-196.

ZIEGLER, P. A. & MAATSCHAPPIJ'S-GRAVENHAGE, K. N. P. 1982. Geological atlas of western and central Europe.

ZONENSHAĬN, L. P., KUZ'MIN, M. I. & NATAPOV, L. M. 1990. *Geology of the USSR: a plate-tectonic synthesis*, American Geophysical Union.

http://www.bbc.co.uk/nature/history_of_the_earth/Triassic

PLATE 1

Scale bars represent 10 μm.

A *Micrhystridium* sp.

B *Brachisaccus* sp.

C *Lunatisporites* sp.

D *Botryococcus* sp

E *Baltisphaeridium* sp.cluster

F *Cymatiosphaera* sp.

G Foraminifera test lining

H *Tasmanites* sp.

I *Calamospora* sp.

J Tetrad of *Duplicisporites* sp.

K *Patinasporites* sp.

L *Triadispora* sp.

M cf. *Vesicaspora fuscus*

N *Enzonalasporites* sp.

O *Kraeuselisporites* sp.

P *Cymatiosphaera* sp.

Q *Tasmanites* sp.

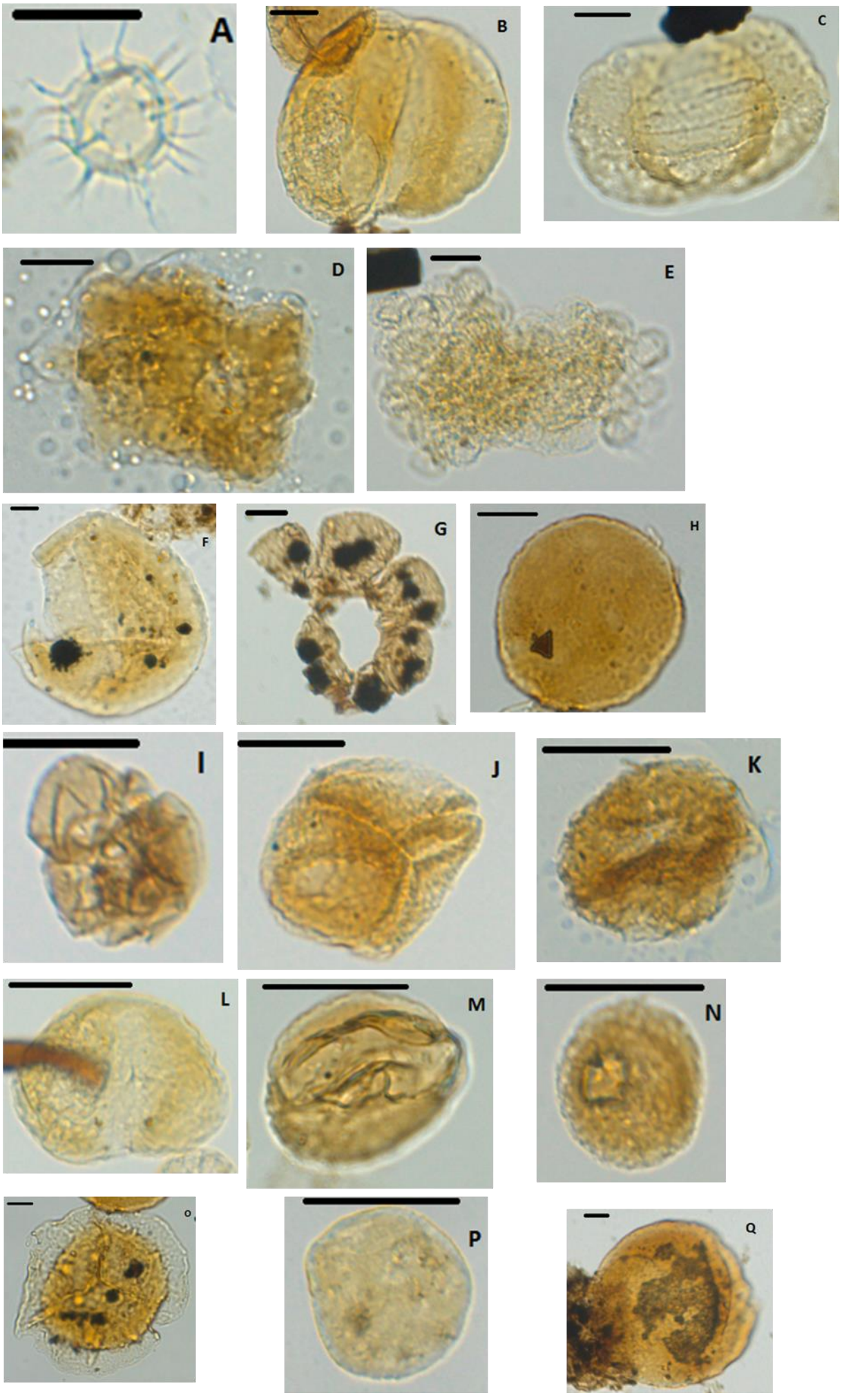
A
B
C
D
E
F
G
H
I
J
K
L
M
N
O
P
Q

A. Palynofacies data & $\delta^{13}C_{org}$ values

Sample:	Depth	Resin	AOM heterogenous	AOM homogenous	Charcoal equidim ensional	Charcoal lath shaped	Fungal hyphae	Wood remains	Cuticle remains	Degraded irregular plant cuticles	Degraded plant tissue	Spores	Bisssacate Pollen	Pollen	Acritarchs	Prasinophytes	Botryococcus	Foraminiferal	Scolecodonts	SUM	δ^{13}COrg
SBG241	415	4	22	1	30	10	0	42	0	153	2	2	19	45	12	0	0	0	0	340	-24,5
SBG242	418	0	22	0	28	15	0	32	0	137	0	3	14	35	5	1	2	0	0	293	-24,34
SBG244	419	0	22	0	19	8	0	36	1	157	3	2	22	48	8	1	0	0	0	325	-24,72
GR20	428,4	1	343	0	11	3	0	15	2	5	0	0	31	31	9	0	0	5	1	454	-26,38
GR18	428,8	2	246	0	3	1	0	12	1	0	0	0	13	11	15	0	0	2	0	303	-26,29
GR16	429,4	4	54	2	30	5	0	51	4	10	0	2	17	32	6	1	0	1	0	216	-25,14
GR14	429,8	1	245	0	10	3	2	10	3	1	0	0	15	20	14	0	0	3	0	324	-26,03
GR12	430,3	2	210	0	4	2	0	7	1	0	0	0	7	9	20	0	0	3	0	263	-26,03
GR10	430,8	5	175	0	21	5	0	14	4	6	0	0	41	36	2	0	0	0	0	307	-25,21
GR8	431,2	2	45	0	64	17	0	27	20	19	0	3	39	76	7	0	0	0	0	318	-27,19
GR7	431,5	3	167	0	12	1	0	35	1	1	0	0	28	75	2	0	0	0	0	321	-26,42
GR6	431,6	1	271	0	7	1	1	11	0	1	0	0	6	21	7	5	0	0	0	331	
GR2	432,2	11	266	0	30	2	0	48	18	4	0	0	16	43	5	4	0	0	0	445	-26,32
GR1	432,9	1	375	0	47	6	0	36	8	1	0	0	21	66	6	3	0	0	0	568	-26,08
STB1	434,9	0	205	0	1	0	0	14	0	0	0	0	1	23	16	3	0	0	0	262	-27,29
STB3	436,4	2	153	0	2	1	0	39	0	0	0	0	6	54	12	1	0	0	0	269	-26,2
STB5	437,4	2	91	0	6	1	0	127	1	2	0	0	1	28	7	2	0	0	0	266	-23,62
STB8	439,3	2	46	0	42	1	0	140	10	20	0	0	1	4	1	0	0	0	0	264	-23,71

B. Geochemical data

Job	Analysis	Labcode	Sample	Depth	Qty - (mg)	S1 - (mg/g)	S2 - (mg/g)	PI	Tmax(°C)	TpkS2(°C)	S3CO - (mg/g)	S3'CO - (mg/g)	S3 - (mg/g)	S3' - (mg/g)	PC(%)	RC(%)	TOC(%)	HI	OI	pyroMINC(%)
2015-003	15003001a.r00	2015003001a	GR1	432,9	27,9	0,13	10,73	0,01	427	464	0,40	2,10	1,13	9,20	0,99	4,3582	5,3482	201	21	0,30
2015-003	15003002a.r00	2015003002a	GR2	432,2	37,9	0,07	1,58	0,04	436	473	0,19	1,00	1,87	9,40	0,22	2,0313	2,25125	70	83	0,28
2015-003	15003003a.r00	2015003003a	GR5	431,7	36,8	0,06	2,32	0,03	429	466	0,11	1,40	0,92	6,80	0,26	4,63	4,89	47	19	0,22
2015-003	15003004a.r00	2015003004a	GR7	431,5	29,4	0,03	0,44	0,07	439	476	0,07	0,60	1,11	10,00	0,09	1,1659	1,25588	35	88	0,29
2015-003	15003005a.r00	2015003005a	GR8	431,2	34,4	0,04	0,76	0,05	426	463	0,09	0,70	1,03	6,20	0,11	0,5527	0,66266	115	155	0,18
2015-003	15003006a.r00	2015003006a	GR10	430,8	36,8	0,04	1,93	0,02	432	469	0,21	0,40	0,54	11,70	0,20	1,0547	1,25466	154	43	0,33
2015-003	15003007a.r00	2015003007a	GR12	430,3	34,6	0,04	1,49	0,02	431	468	0,09	0,60	0,56	7,20	0,16	1,0789	1,23888	120	45	0,21
2015-003	15003008a.r00	2015003008a	GR14	429,8	34,2	0,05	0,66	0,07	427	464	0,10	0,70	0,66	8,00	0,10	0,8191	0,91912	72	72	0,23
2015-003	15003009a.r00	2015003009a	GR16	429,4	33,7	0,04	0,36	0,10	430	467	0,06	0,40	0,44	3,20	0,06	0,6103	0,67032	54	66	0,10
2015-003	15003010a.r00	2015003010a	GR18	428,8	33,8	0,03	0,96	0,03	428	465	0,12	0,50	0,82	4,80	0,12	1,0222	1,14218	84	72	0,14
2015-003	15003011a.r00	2015003011a	GR20	428,4	29,6	0,08	0,96	0,08	429	466	0,12	0,70	0,95	9,80	0,13	1,196	1,32599	72	72	0,28
2015-003	15003012a.r00	2015003012a	GR22	427,6	33,0	0,02	0,76	0,02	428	465	0,12	0,60	0,60	11,10	0,10	1,0008	1,10077	69	55	0,32
2015-003	15003013a.r00	2015003013a	GR24	427,1	36,9	0,03	0,47	0,06	429	466	0,09	0,50	0,54	4,50	0,07	0,8563	0,92631	51	58	0,13
2015-003	15003014a.r00	2015003014a	GR26	426,7	36,8	0,03	0,42	0,06	430	467	0,21	0,30	0,52	3,00	0,07	0,9501	1,02006	41	51	0,09
2015-003	15003015a.r00	2015003015a	GR X	424,0	37,8	0,02	0,34	0,07	429	466	0,26	0,30	0,66	3,30	0,07	0,9132	0,98322	35	67	0,10
2015-003	15003016a.r00	2015003016a	ME 001	441,3	39,9	0,02	0,06	0,27	427	464	0,03	0,20	0,74	7,40	0,03	0,186	0,21595	28	343	0,21
2015-003	15003017a.r00	2015003017a	ME 003	450,9	73,4	0,06	0,30	0,16	434	471	0,10	0,20	0,77	6,70	0,06	0,3908	0,45084	67	171	0,19
2015-003	15003018a.r00	2015003018a	STB1	434,9	25,8	0,23	9,40	0,02	427	464	0,46	2,60	1,77	12,20	0,92	14,212	15,132	62	12	0,39
2015-003	15003019a.r00	2015003019a	STB3	436,4	14,1	0,34	17,87	0,02	430	467	1,18	4,20	3,96	20,60	1,76	8,1283	9,88831	181	40	0,65
2015-003	15003020a.r00	2015003020a	STB5	437,4	26,6	0,06	0,59	0,09	426	463	0,32	0,50	1,44	22,60	0,12	1,7815	1,90149	31	76	0,63
2015-003	15003021a.r00	2015003010a	STB8	439,3	80,9	0,03	0,10	0,23	262	299	0,03	0,30	0,87	16,20	0,04	0,5732	0,61322	16	142	0,45
2015-003	15003022a.r00	2015003022a	SBG 2-33	407,0	63,0	0,03	0,30	0,08	434	471	0,06	0,30	0,40	6,60	0,05	0,7608	0,8108	37	49	0,19
2015-003	15003023a.r00	2015003023a	SBG 2-35	409,0	67,4	0,05	0,48	0,09	436	473	0,05	0,30	0,37	11,30	0,06	0,8679	0,92785	52	40	0,31
2015-003	15003024a.r00	2015003024a	SBG 2-37	411,0	73,7	0,01	0,31	0,03	434	471	0,05	0,30	0,50	6,10	0,05	0,759	0,80905	38	62	0,17
2015-003	15003025a.r00	2015003025a	SBG 2-39	413,0	89,1	0,03	0,25	0,12	432	469	0,05	0,20	0,41	4,50	0,04	0,6658	0,70575	35	58	0,13
2015-003	15003026a.r00	2015003026a	SBG 2-41	415,0	58,7	0,04	0,35	0,10	433	470	0,09	0,30	0,76	6,30	0,06	0,8252	0,88516	40	86	0,18
2015-003	15003027a.r00	2015003027a	SBG 2-42	417,0	69,0	0,01	0,28	0,05	436	473	0,19	0,20	0,74	3,50	0,06	0,7265	0,78647	36	94	0,10
2015-003	15003028a.r00	2015003028a	SBG 2-44	419	71,6	0,03	0,37	0,1	434	471	0,04	0,2	0,24	8,2	0,05	0,761	0,8105	46	30	0,23